Towards unified drag laws for inertial flow through fibrous materials

K. Yazdchi[*] and S. Luding

Multi Scale Mechanics (MSM), Faculty of Engineering Technology,
University of Twente, P.O. Box 217, 7500 AE Enschede, The Netherlands

Abstract:

We give a comprehensive survey of published experimental, numerical and theoretical work on the drag law correlations for fluidized beds and flow through porous media, together with an attempt of systematization. Ranges of validity as well as limitations of commonly used relations (i.e. the Ergun and Forchheimer relations for laminar and inertial flows) are studied for a wide range of porosities. The pressure gradient is linear in superficial velocity, U for low Reynolds numbers, Re, referred to as Darcy's law. Here, we focus on the non-linear contribution of inertia to the transport of momentum at the pore scale, and explain why there are different non-linear corrections on the market.

From our fully resolved finite element (FE) results, for both ordered and random fibre arrays, *(i)* the weak inertia correction to the linear Darcy relation is third power in U, up to small Re~1-5. When attempting to fit our data with a particularly simple relation, *(ii)* a non-integer power law performs astonishingly well up to the moderate Re~30. However, e.g. for randomly distributed arrays, *(iii)* a quadratic correction performs quite well as used in the Forchheimer (or Ergun) equation, from small to moderate Re.

Finally, as main result, the macroscopic properties of porous media are related to their microstructure (arrangement) and porosity. All results (Re<30) up to astonishingly large porosity, ε~0.9, to scale with Re_g, i.e., the gap Reynolds number that is based on the average second nearest neighbor distances. This universal result is given as analytical closure relation, which can readily be incorporated into existing (non)commercial multi-phase flow codes. The universal curve actually can be fitted with a non-integer power law (better than ~1% deviation), but also allows to define a critical Re_{gc}~1, below which the third power holds and above which a correction with second power fits the data considerably better.

Keywords: Inertial flow; Fibrous porous media; FEM; Microstructure; Drag law

---

[*] - Corresponding author: K. Yazdchi (k.yazdchi@utwente.nl), S. Luding (s.luding@utwente.nl), Tel: +31534893345

1. Introduction

The transport phenomena in porous media have been the focus and interest of numerous studies for the past decades. This interest stems from a wide range of applications in such industries as chemical, mechanical, geological, environmental, petroleum, etc [1-5]. The flow conditions encountered are broad enough to cover a wide range of Reynolds numbers (Re) and porosities. In practice, three distinct flow regimes are commonly defined in literature in terms of Reynolds number: (i) stationary Darcy or creeping flow, (ii) steady, laminar inertial flow and (iii) unsteady chaotic/turbulent flow regimes. As an example, creeping flows (i.e., $Re \ll 1$) may be encountered in ground water flows, composites manufacturing and filtering, whereas inertial flows are found in applications such as heat exchangers or packed bed chemical reactors. Highly turbulent flow is expected, e.g., in gas-fluidized beds. The flow regimes studied in this paper are limited to regimes (i) and (ii). Several macroscopic parameters are often needed to complete coarse grained models that are employed to describe such applications. This has motivated the research in the development of relationships to describe macroscopic parameters, such as permeability and inertial coefficients, for different kinds of porous media at various porosities and flow regimes.

Most porous media are particulate, but some are composed of long particles/fibres and, therefore, may be considered as fibrous media. They are encountered in a variety of modern technology applications, predominantly in the manufacturing of fibre-reinforced composites, with extensive use in the aerospace and automobile industries.

With the recent progress in computational and numerical tools, one can now perform detailed calculations of heavily loaded, fluid-particle flows, based on two-fluid models (TFM) and/or the discrete particle method (DPM) [3, 4]. However, these methods require the knowledge of several constitutive laws (i.e. the interphase momentum-transfer coefficient of the gas/fluid phase acting on the particles/solid). Accurate drag laws are a basic requirement in simulations based on DPM or TFM to be successfully used in the design and optimization of industrial processes. Such correlations have a strong dependence on the pore structure and pore-level physics, which generally requires them to be estimated experimentally or through the use of existing empirical relations.

At the macroscopic level and the limit of creeping flow regimes, the pressure gradient ∇p, and the flow rate have a linear relation, known as Darcy's law:

$$-\nabla p = \frac{\mu}{K} U \ , \tag{1}$$

where μ and U are viscosity and superficial velocity, respectively. The proportionality constant K, is called the permeability of the medium, which strongly depends on porosity and microstructure (e.g., fibre/particle shape and arrangement, void connectivity and inhomogeneity of the medium). The effect of several microstructural parameters on macroscopic permeability was investigated for ordered and disordered fibrous media, see Refs. [5-7] and references therein.

Darcy's law was originally obtained from experiments [8] and later formalized using upscaling [9], homogenization [10, 11] and volume averaging [12, 13] techniques. It has been shown that Darcy's law actually represents the momentum equation for Stokes flow averaged over a representative volume element (RVE), implying that it is valid only in the creeping flow regime [14].

The effect of fluid inertia, on the other hand, is a more complex problem, lending itself to numerical rather than analytical treatment. Active research has been dedicated to derive adequate corrections to the linear relationship in Eq. (1) from numerical, theoretical, and experimental points of view. Koch and Ladd [15] and Hill et al. [16] simulated moderate Reynolds number flows through periodic and random arrays of aligned cylinders and spheres using the Lattice Boltzmann Method (LBM). They showed that the inertial term made a transition from linear to quadratic in random arrays. The inertial effect became smaller at the volume fraction approaching close packing due to increased drag forces through the narrowing channels. The experimentation that proved this nonlinear relation was carried out by Forchheimer [17], who indicated that there exists a quadratic term of the flow rate when the Reynolds number is sufficiently high. While the LBM has been successfully applied for the simulation of porous media flow in the creeping regime [18-20], its applicability for high Reynolds numbers has been the subject of more speculation and debate due to selection of parameters, resolution and the necessity to reduce compressibility effects [21, 22]. Andrade et al. [23] demonstrated that, for a 2D disordered porous structure at high porosity, the incipient departure from the Darcy law

could be observed already in the steady, laminar inertial flow before arriving at turbulent/chaotic regime.

To date, mainly empirical relations, such as by Ergun [24], and their components, the Carman-Kozeny (viscous term) and Burke-Plummet (inertial term) equations, have proved to be quite useful [25, 26]. Liu et al [27] devised a semi-empirical formula for the pressure drop, which incorporates the tortuosity, the curvature ratio and the variation of the pore cross-sectional area. Jackson and James [28] conducted a comprehensive review of the literature on a variety of theoretical models and presented a large collection of experimental data for both natural and synthetic fibrous media. A recent discrete particle study by Bokkers et al. [29] showed that, with respect to bubble formation in fluidized beds, the drag relations derived from the lattice-Boltzmann simulations of Hill et al. [16] yielded better agreement with the experimental observations than the traditional Ergun and Wen & Yu [30] correlations. While the latter relation remains the most widely used in chemical engineering, an accurate description for the interphase momentum transfer has been a subject of debate. This has motivated the research in the development of more accurate relationships to describe the macroscopic momentum transfer in terms of microscopic pore-scale parameters.

Most of the previously obtained drag laws are only valid for 3D, spherical packed beds. Although the drag relation for 2D fibrous materials and 3D packed beds are quite different (for instance in 2D the drag diverges in the limit of close packing), our attempt is to check the validity of those relations for 2D systems. We establish the relationship between microscopic and macroscopic properties of fibrous media by conducting a systematic study using numerical simulations based on the finite element method (FEM). In order to get a better understanding of the state-of-the-art on non-Darcy flow, literature concerning the theoretical basis of the Forchheimer equation and experimental work on the identification of flow regimes is reviewed in Section 2. After presenting the numerical method used to compute the permeability and inertial coefficients, results are discussed in Section 3. The steady state fluid flow across uni-directional arrays of cylinders are considered, for both ordered and disordered configurations. Computations were carried out with special attention to high accuracy (resolution) in order to investigate the existence of the different regimes and the corresponding scaling laws. The effects of

several structural parameters, namely porosity, disorder and fibre-shape on the flow behavior at various regimes are discussed in detail. The paper is concluded in Section 4 with a summary and outlook for future work.

2. Theoretical background

Flows in porous media can be studied at either microscopic or macroscopic scales. For the former scale the flow through individual pores is computed by solving the mass and momentum equations (i.e., the Navier–Stokes (NS) equation) numerically, whereas for the latter a continuum description is usually adopted based on volume averaging of the equations pertaining to microscopic scales. The linking of these two descriptions constitutes the well known scaling-up problem, which usually provides macroscopic properties in terms of the permeability, i.e., the ability of a porous material to transmit fluids. Although the permeability can, in principle, provide quantitative correlations between morphological features of pore geometry and its capacity to transmit liquid, its values depend on many factors such as porosity, typical length scale of pores, grain size distribution, shape, anisotropy and tortuosity of pore connections, see Refs. [5-7] and references therein. Therefore, the permeability determined either analytically or empirically for porous media with complex structures involves considerable uncertainty – one can not determine microscopic properties only from the macroscopic permeability.

As mentioned before, Darcy's law is the most widely used empirical correlation for the calculation of the pressure drop across a homogeneous, isotropic, unbounded and non-deformable porous medium. It is strictly valid for incompressible and isothermal Stokes flow (Re = 0) of Newtonian fluids. However, it is usually applicable in engineering applications for Re < 1, defined by $Re = \rho U l / \mu$ where l and ρ are the typical pore size of the structure and density of the fluid, respectively. Darcy's law, since it lacks, among other reasons, the flow inhomogeneity/variability[1], is not valid at the interface of a porous medium-solid or porous medium-free flow. Brinkman [31] added a diffusion-type term to the Darcy's law, leading to

$$-\nabla p = \frac{\mu}{K}U - \mu \nabla^2 U \ .$$ (2)

---

[1] It can not account for the no-slip boundary condition at the solid boundary of the porous medium.

Brinkman's equation is, like Darcy's law, inertia-free and hence valid only for creeping flows. Recently, Auriault [32] discussed the validity and limitations of Brinkman's equation for "classical" porous media, swarms of low concentration particles and fibrous media at high porosities.

In the continuum approach one describes mass and momentum balance equations at macroscopic scale, using a specific averaging procedure. Therefore, the major difficulty resides in an adequate determination of the averaging domain. Following a continuum approach, Hassanizadeh and Gray [33] developed a set of equations to describe the macroscopic behavior of fluid flow through porous media. Linearization of these equations yields a Darcy equation at low velocities.

Although the physical nature of the deviation from Darcy's law is still unclear and may have several reasons (probably acting together), empirical relationships allow correlating the pressure drop and average fluid velocity in porous media. To account for the non-linear behavior of the flow in porous media, Forchheimer [17] added a quadratic velocity term to represent the microscopic inertial effect, and corrected the Darcy equation into the Forchheimer equation

$$-\nabla p = \frac{\mu}{K}U + \beta\rho U^2 \; , \tag{3}$$

where the constant, β is referred to as the non-Darcy coefficient which, like permeability, is an empirical value that depends on the micro-parameters of porous media. Similar to Darcy's law, Forchheimer's law was originally postulated heuristically to account for the experimental data. However, during the past decades there has been an effort to derive it from first principles. Some of the techniques used are matched asymptotic expansions [34], the capillary model [35], hybrid mixture theory [36] and volume averaging [12, 37, 38]. The physical justification of the quadratic nature of the correction was supported either by intuition or by dimensional analysis and the analogous turbulent kinetic energy loss in straight tubes [39]. Moutsopoulos et al. [40] investigated phenomenological relations for the Forchheimer equation experimentally and theoretically for both homogeneous and heterogeneous media. Based on homogenization approach, Chen et al. [41] claim that the nonlinear filtration law is quadratic. By generalizing the Forchheimer

equation, Ergun obtained the following empirical relation for homogenous, packed beds of randomly distributed spheres:

$$-\nabla p = A\frac{(1-\varepsilon)^2}{\varepsilon^3}\frac{\mu U}{d^2} + B\frac{(1-\varepsilon)}{\varepsilon^3}\frac{\rho U^2}{d} \quad , \tag{4}$$

where d is the average diameter of the particles in the domain and ε is the porosity[2]. After analysis of a large quantity of experimental data, Ergun concluded that their best representation could be obtained with $A = 150$ and $B = 1.75$. However, in subsequent studies these values have been found to vary considerably with shape, porosity and Re number [42, 43]. In particular, after testing the Ergun equation using many more data than ever before, MacDonald et al. [42] found that $A = 180$, and $B = 1.8$ (smooth particles) or 4.0 (rough particles) give the best fits to all of the involved data. Besides the Ergun equation, there are correlations using the non-dimensional particle friction factor, f_p, through the following definition

$$f_p = \frac{-\nabla p d}{\rho U^2}. \tag{5}$$

By combining Eqs. (5) and (3), the Forchheimer equation can be written as:

$$f_p = \frac{1}{\text{Re}\,K^{'}} + \beta^{'}, \tag{6}$$

where $\text{Re} = \rho U d / \mu$, $K^{'} = K/d^2$ and $\beta^{'} = \beta d$ are the Reynolds number (based on diameter d), the normalized permeability and the modified non-Darcy coefficient, respectively. The latter two, $K^{'}$ and $\beta^{'}$, can be considered as the non-dimensional, macroscopic viscous and inertial coefficients with the beauty of a constant friction factor in the inertial regime. Looking at the literature, we found several definitions and relations between friction factor and Re (or sometimes pressure gradient and U) which makes it difficult to make one-to-one comparison. Table 1 summarizes all theses definitions and their relations.

In Table 2, the available modifications of Ergun's equation and their range of validity are listed as function of the particle Re number, $\text{Re}_p = \text{Re}/(1-\varepsilon)$. Therefore, most equations have the typical porosity term, $(1-\varepsilon)/\varepsilon^3$, for low Re, with various different constants

---

[2] Comparing Eqs. (3) and (4), one can relate the parameters A, B, and ε to K and β.

and strongly varying further terms [42, 60, 62-64, 67-69] representing the effect of wall, shape, etc. A few of the equations have non-linear corrections also in the first term [54, 59, 66], and the last class are sums of several powers of Re used to fit into available experimental/numerical data [52, 53, 61]. A more complete list of correlations for the viscous term, i.e. at low Re numbers, of 2D fibrous materials can be found in Ref. [5]. Recently, Barree and Conway [44] conducted experiments suggesting that Forchheimer's equation is only valid over a limited range of velocities. Derivations using volume averaging was undertaken by Ruth and Ma [12], and Whitaker [38]. However, Ruth and Ma [12] explain that microscopic inertial effects are neglected in volume- averaging techniques and therefore cannot be used to derive a macroscopic law. They point out that the Forchheimer equation is not unique, and any number of polynomials could be used to describe nonlinear behavior due to inertia in non-laminar flow. This is confirmed in Bourgeat et al. [45], where the nonlinear filtration law is obtained as an infinite series in integer powers of the local Reynolds number. More recently, Balhoff et al. [46] used the method of homogenization to develop a general polynomial filtration law for low Reynolds numbers. In Marušic–Paloka and Mikelic [47], the existence, uniqueness and regularity of general non-local filtration law was rigorously established in the homogenization limit when the pore size tends to zero.

Table 1: Various definitions and relations between friction factors and Re (or pressure gradient and superficial velocity, U)

Friction factor – Re (or pressure gradient – U) relation	Comment
$-\nabla p \sim U$	Linear Darcy's law for creeping flow, Eq. (1)
$-\nabla p \sim U - \nabla^2 U$	Brinkman's equation for creeping flow at high porosities, Eq. (2)
$-\nabla p \sim U + U^2$	Forchheimer (Ergun) equation, quadratic correction to Darcy's law, Eq. (3)
$-\nabla p \sim U + U^3$	Cubic correction to Darcy's law at small Re, Eq. (7)
$f_p \sim -\nabla p / U^2 \sim \mathrm{Re}^{-1} + \beta'$	Particle friction factor as function of Re. β' is the inertial, porosity dependent parameter, see Table 2
$f' \equiv f_p \mathrm{Re} \sim -\nabla p / U \sim \alpha' + \mathrm{Re}^\lambda$	Non-integer, λ, power law fit, used in this paper, Eq. (8). α' is the viscous, porosity dependent term
$f^* \sim f' - \alpha' \sim \mathrm{Re}_g^\lambda$	Isolated inertial term used for scaling the data in Appendix D, Re$_g$ is "gap" Re number

One of the important observations from Wodié and Levy [48], Mei and Auriault [11], and Rasoloarijaona and Auriault [49] was that for an isotropic porous medium, the quadratic terms cancel and one has a cubic filtration law given by

$$-\nabla p = \frac{\mu}{K}U + \frac{\gamma^* \rho^2}{\mu}U^3 \quad \Rightarrow f_p = \frac{1}{\operatorname{Re} K'} + \gamma^* \operatorname{Re}, \tag{7}$$

where γ^* is a porosity dependent dimensionless parameter. This observation is confirmed analytically and numerically in [50] and for periodic two-dimensional arrays of cylinders arranged in a regular pattern in [51]. In most cases, the cubic law is only valid at very low velocities (Re < 1, where Darcy's law is approximately valid anyway), and the quadratic Forchheimer equation appears applicable at higher, moderate velocities (1<Re<10). Nonetheless, these findings are significant because they suggest that any power law with integer power, like in the Forchheimer equation, may not be universal and only valid in a limited range of velocities and porosities.

Despite extensive previous work, our understanding of the physical reasons for non-Darcy flow is incomplete. To better understand the microscopic origin of these correlations, we conduct a set of FE simulations on both ordered and disordered arrays of cylinders in a wide range of Reynolds numbers in the next section.

Table 2: Available modifications of the Ergun equation in terms of the particle friction factor, f_p and the particle Reynolds number $\operatorname{Re}_p = \operatorname{Re}/(1-\varepsilon) = \dfrac{\rho U d}{(1-\varepsilon)\mu}$. Unless explicitly stated, the relations are valid for 3D, disordered systems.

Author	f_p	Range of validity
Ergun [24]	$\left(\dfrac{1-\varepsilon}{\varepsilon^3}\right)\left(\dfrac{150}{\operatorname{Re}_p}+1.75\right)$	$\varepsilon < 0.8$
MacDonald et al. [42]	$\left(\dfrac{1-\varepsilon}{\varepsilon^3}\right)\left(\dfrac{180}{\operatorname{Re}_p}+B'\right)$	$B'=1.8,$ smooth particles $B'=4,$ rough particles
Rose [52]	$1000\operatorname{Re}_p^{-1}+60\operatorname{Re}_p^{-0.5}+12$	Mean value of $\operatorname{Re}_p \cong 140$
Rose and Rizk [53]	$1000\operatorname{Re}_p^{-1}+125\operatorname{Re}_p^{-0.5}+14$	$1000 < \operatorname{Re}_p < 6000$
Hicks [54]	$6.8\dfrac{(1-\varepsilon)^{1.2}}{\varepsilon^3}\operatorname{Re}_p^{-0.2}$	$500 < \operatorname{Re}_p < 60000$

Tallmadge [55]	$$\frac{150}{\mathrm{Re}_p}\frac{(1-\varepsilon)^2}{\varepsilon^3}+\frac{4.2(1-\varepsilon)^{1.166}}{\varepsilon^3}\mathrm{Re}_p^{-1/6}$$	$0.1<\mathrm{Re}_p<10^5$
Lee and Ogawa [56]	$$\frac{1}{2}\left(\frac{12.5}{\varepsilon^3}(1-\varepsilon)^2\right)\left(29.32\,\mathrm{Re}_p^{-1}+1.56\,\mathrm{Re}_p^{-n}+0.1\right)$$ $$n=0.352+0.1\varepsilon+0.275\varepsilon^2$$	$1<\mathrm{Re}_p<10^5$
Kürten et al. [57]	$$\left(\frac{25}{4\varepsilon^3}(1-\varepsilon)^2\right)\left(21\,\mathrm{Re}_p^{-1}+6\,\mathrm{Re}_p^{-0.5}+0.28\right)$$	$0.1<\mathrm{Re}_p<4000$
Montillet et al. [58]	$$\alpha\left(1000\,\mathrm{Re}_p^{-1}+60\,\mathrm{Re}_p^{-0.5}+12\right)$$ $$\alpha=0.061\left(\frac{1-\varepsilon}{\varepsilon^3}\right)\left(\frac{D}{d}\right)^{0.2}$$	$10<\mathrm{Re}_p<2500$, D: bed diameter
Özdinç et al. [59]	$$69.785\left(\frac{d}{L}\right)\left(\mathrm{Re}_p\left(\frac{d}{L}\right)\varepsilon^7\right)^{-0.4733}$$	$675<\mathrm{Re}_p<7772$
Ozahi et al. [60]	$$\left(\frac{1-\varepsilon}{\varepsilon^3}\right)\left(\frac{D}{d}\right)\left(3\times10^{-5}\,\mathrm{Re}_p-66.487\,\mathrm{Re}_p^{-1}+0.1539\right)$$	$800<\mathrm{Re}_p<8000$, D: bed diameter
Gibilaro et al. [61]	$$\left(17.3\,\mathrm{Re}_p^{-1}+0.336(1-\varepsilon)\right)\varepsilon^{-4.8}$$	In fluidized suspensions
Benyahia et al. [62]	$$\frac{180(1-\varepsilon)}{\mathrm{Re}_p\,\varepsilon^3}+9F_3(1-\varepsilon)$$ $$F_3=0.0673+0.212(1-\varepsilon)+0.0232\varepsilon^{-5}$$	$\varepsilon<0.6$, $\mathrm{Re}_p>\dfrac{2F_3}{F_1(1-\varepsilon)}$, $F_1=0.11+0.00051e^{11.6(1-\varepsilon)}$
Molerus [63]	$$\left(\frac{1-\varepsilon}{\varepsilon^2}\right)\left(\left(\frac{18}{1-\varepsilon}+\frac{49.5}{\varepsilon}\right)\mathrm{Re}_p^{-1}+\frac{0.69}{\varepsilon^2}\right)$$	$\varepsilon<0.7$
Kovács [64]	$$\left(\frac{1-\varepsilon}{\varepsilon^3}\right)\left(\frac{144}{\mathrm{Re}_p}+2.4\right)$$	$10<\mathrm{Re}_p(1-\varepsilon)<100$
Kadlec and Knight [65]	$$\left(\frac{1-\varepsilon}{\varepsilon^3}\right)\left(\frac{255}{\varepsilon^{0.7}(1-\varepsilon)\mathrm{Re}_p}+2\right)$$	In fluidized suspensions
Foscolo et al. [66]	$$\left(\frac{1-\varepsilon}{\varepsilon^{4.8}}\right)\left(\frac{17.3}{\mathrm{Re}_p(1-\varepsilon)}+0.336\right)$$	Laminar and turbulent regimes, $\varepsilon>0.4$

Mehta and Hawley [67]	$\left(\dfrac{1-\varepsilon}{\varepsilon^3}\right)M\left(\dfrac{150}{\mathrm{Re}_p}M+1.75\right)$	$M=1+\dfrac{2d}{3D(1-\varepsilon)}$, D: bed diameter
Du Plessis [68]	$\left(\dfrac{1-\varepsilon}{\varepsilon^3}\right)\left(\dfrac{A}{\mathrm{Re}_p}+\varepsilon^2/\left(1-(1-\varepsilon)^{2/3}\right)^2\right)$, $A=\dfrac{41\varepsilon^2}{(1-\varepsilon)^{2/3}\left(1-(1-\varepsilon)^{1/3}\right)\left(1-(1-\varepsilon)^{2/3}\right)}$	Packed bed of spherical particles
Reichelt [69]	$\left(\dfrac{1-\varepsilon}{\varepsilon^3}\right)\left(\dfrac{K_1 A_w^2}{\mathrm{Re}_p}+B_w\right)$, $A_w=1+\dfrac{2}{3(D/d)(1-\varepsilon)}$, $B_w=\dfrac{1}{\left(k_1(d/D)^2+k_2\right)^2}$	Spheres: $K_1=154$, $k_1=1.5$, $k_2=0.88$ Cylinders: $K_1=190$, $k_1=2$, $k_2=0.77$ D: bed diameter
Martin et al. [70]	$b\varepsilon^{-n}\left(\mathrm{Re}_p\,\dfrac{\sqrt{K}}{d}(1-\varepsilon)\right)^m\dfrac{d}{\sqrt{K}}$	Square and triangular fibre arrays, with $0.8<\varepsilon<0.99$ and $3<\mathrm{Re}_p<160$. The n, m and b are fitting parameters.
Papathanass iou et al. [26]	$\dfrac{d^2}{\mathrm{Re}_p\,K(1-\varepsilon)}+0.08\dfrac{(1-\varepsilon)d}{\varepsilon\sqrt{K}}$	Square and hexagonal fibre arrays, with $0.3<\varepsilon<0.6$ and $0<\mathrm{Re}_p<400$
Tamayol et al. [71]	$\dfrac{d^2}{\mathrm{Re}_p\,K(1-\varepsilon)}+\dfrac{(a+b\varepsilon)^{-1/c}d}{\sqrt{K}}$	1D, 2D and 3D ordered fibrous media in the range of $0.35<\varepsilon<0.95$ and $0.01<\mathrm{Re}_p<4000$. The a, b and c are fitting parameters.

Koch et al. [15]	(a) $\dfrac{k_1}{\mathrm{Re}_p} + k_2 \, \mathrm{Re}_p$ (b) $\dfrac{c_1}{\mathrm{Re}_p} + c_2$	(a) For both periodic and random fiber arrays at Re<1; k_1 and k_2 are porosity dependent parameters. (b) For random arrays at Re>5 (similar to Ergun relation); c_1 and c_2 are porosity dependent parameters.
Tanino and Nepf [72]	$\dfrac{\alpha_0}{\mathrm{Re}_p} + \alpha_1$	Randomly distributed, rigid, emergent circular cylinders in the range of $0.65 < \varepsilon < 0.9$ and $70 < \mathrm{Re}_p < 6850$ (similar to Ergun relation). The α_0 and α_1 are porosity dependent fitting parameters.

3. Numerical results

This section is dedicated to the finite element (FE) based model simulations of both ordered and disordered fibre arrays at various porosities and flow regimes. Alternative to the FE method like the lattice Boltzmann method (LBM) can also deal with complex pore geometries and boundary conditions in the inertial regime, but are discussed and compared elsewhere [22]. The results on the friction factor (both the viscous and inertial components) as function of porosity, structure, shape, etc., are presented and discussed.

3.1. Ordered structure

We start the analysis with the case of a 2D regular periodic array of cylinders, perpendicular to the flow direction, as shown in Fig. 1. These models rely on the assumption that the porous media is periodic and thus can be divided into unit cells that are then also representative volume elements (RVE). The friction factor is then determined by modeling the flow through these, more or less, idealized cells.
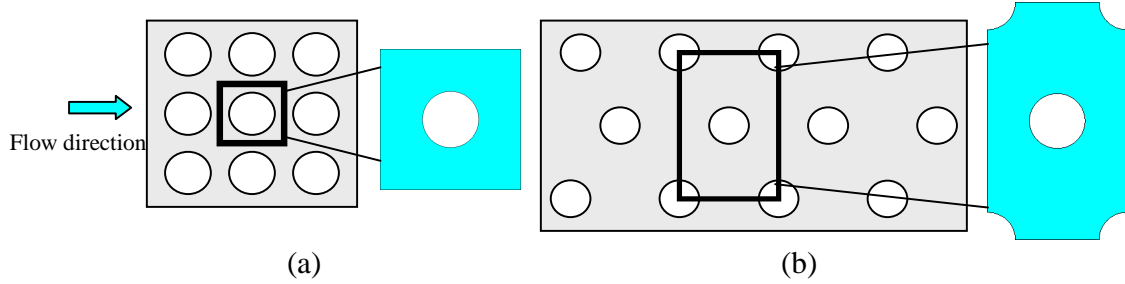
Figure 1: The geometry of the unit cells used for (a) square and (b) hexagonal configurations.

3.1.1 Computational method and boundary conditions

The FE software ANSYS$^{®}$ is used to calculate the superficial velocity, U, from the results of our computer simulations as $U = \dfrac{1}{A} \int_{A_f} u dA$, where A, A_f and u are the total area of the unit cell, area of the fluid and intrinsic fluid velocity, respectively. On the flow domain, the steady state NS equations combined with the continuity equations were discretised into an unstructured, triangular element. They were then solved using segregated, sequential solution algorithm. The developed matrices from assembly of linear triangular elements are then solved based on a Gaussian elimination algorithm. Some more technical details are given in Refs. [5-7]. The mesh size effect is examined by comparing the simulation results for different resolutions (data not shown here). At the left and right pressure- and at the top and bottom periodic-boundary conditions are applied. No-slip boundary conditions, i.e., zero velocity are applied on the surface of the particles/fibres. Computations were performed for Reynolds numbers $10^{-5} < \text{Re} < 30$ and porosity $0.3 < \varepsilon < 0.9$, assuming that the stationary solution is still physically valid in the upper range of this Reynolds numbers.

3.1.2 Generalized Forchheimer equation

The validity of the Forchheimer equation for ordered structures (namely square and hexagonal configuration) is studied in this section. A generalized non-dimensional form

of the Forchheimer Eq. (3) can be derived by postulating a power law and multiplying the friction factor by Re, so that:

$$-f^{'} = \frac{1}{K^{'}} + \gamma \left(\frac{U}{U^{*}} \right)^{\lambda} \equiv \frac{1}{K^{'}} + \gamma \, \mathrm{Re}^{\lambda} \tag{8}$$

where $f^{'} = d^{2}\nabla p/(\mu U) \equiv f_{p}\,\mathrm{Re}$ and $U^{*} = \mu/(\rho d)$ are, by definition, modified friction factor and scaled velocity, respectively. The normalized permeability $K^{'} = K/d^{2}$ and non-dimensional inertial coefficients λ and γ, in general, depend on the porosity and structure of the medium. The power λ represents the deviation from Darcy's regime ($f^{'} = \mathrm{const.}$), so that the non-linear correction can be isolated by studying $-f^{'} - 1/K^{'}$ (as done in the Appendix C). In case of $\lambda = 1$, Eq. (8) reduces to the Ergun equation (Eq. (4) or (6)) with $K^{'} = \varepsilon^{3}/\left(150(1-\varepsilon)^{2}\right)$ and $\gamma = 1.75(1-\varepsilon)/\varepsilon^{3}$. Similarly, for $\lambda = 2$, Eq. (8) reduces to Eq. (7) with $\gamma = \gamma^{*}$. More discussion on the dependence of normalized permeability, $K^{'}$ on porosity and pore-structure for (dis)ordered fibrous medium is given in [5, 6] and references therein. In the following, we rather focus on the influence of micro-structural parameters on the inertial coefficients λ and γ, while $1/K'$ is the low-Re permeability that only depends on porosity.

Fig. 2(a) shows the variation of the modified friction factor as function of normalized velocity, $U/U^{*} \equiv \mathrm{Re}$, for square (red) and hexagonal (blue) configurations for three different porosities. The solid lines represent the best least square fit to the FE data using Eq. (8) with the power as free parameter, while the black dashed line (only one shown at $\varepsilon = 0.6$) represents a fit to the cubic deviation ($\lambda = 2$) from the Darcy regime, which is pretty perfect (99.99% agreement) for Re<3, but strongly overestimates the results for larger Re. As mere examples, the hexagonal structures at $\varepsilon = 0.6, 0.7, 0.8$ correspond to $1/K^{'} = 91.5584, 35.3612, 12.3190$, and $\gamma_{2} = 0.06993, 0.05330, 0.04297$, respectively. Note that for all fits, first the constant, low Re regime is fitted and then the nonlinear correction. Since the cubic correction-term ($\lambda = 2$) – even though perfectly fine for small Re (see Appendix C) – is not a good prediction for larger Re, we will discuss fits with non-integer λ values since they are good approximations up to Re<30.

14

As expected, by increasing the porosity, the normalized permeability, $K^{'}$, increases, i.e. for higher pressure gradients the flow regime changes from Darcy (horizontal line) into inertial (nonlinear) regime. For square configurations the transition starts at lower velocities (i.e. $Re \cong 10$) compared to the hexagonal configuration. Note that in Darcy's regime, the flow is symmetric about both horizontal and vertical axis (not shown here). However, in the inertial regime, due to the non-linear contribution of inertia to the transport of momentum, the symmetry about vertical axes (normal to the flow direction) will break (see section 3.1.4 below, Fig. 5) while the flow is still stationary.

Fig. 2(b) shows the variations of inertial coefficients (i.e. λ and γ) in Eq. (8) as function of porosity for both square and hexagonal configurations. We observe that the power λ is (i) larger than unity and varying between $1 < \lambda < 2$ and (ii) not only depends on porosity but also on structure/arrangements of the particles/fibres. By increasing porosity (i.e. for more dilute systems) the power decreases and approaches the value of unity (i.e. the original quadratic Forchheimer correction, Eq. (3)). Square arrays have larger values of λ compared to hexagonal arrays implying that the transition to inertial regime starts earlier and sharper (see Fig. 2(a)). On the contrary, the pre-factor γ (in the inset) seems to be independent of structure and linearly decreases by increasing porosity as $\gamma \cong 0.8(1-\varepsilon)$. In the appendix A, the quality of the proposed power law fit (Eq. (8)) is compared with the quadratic ($\lambda = 1$) and cubic ($\lambda = 2$) fits at different porosity for both square and hexagonal configurations.
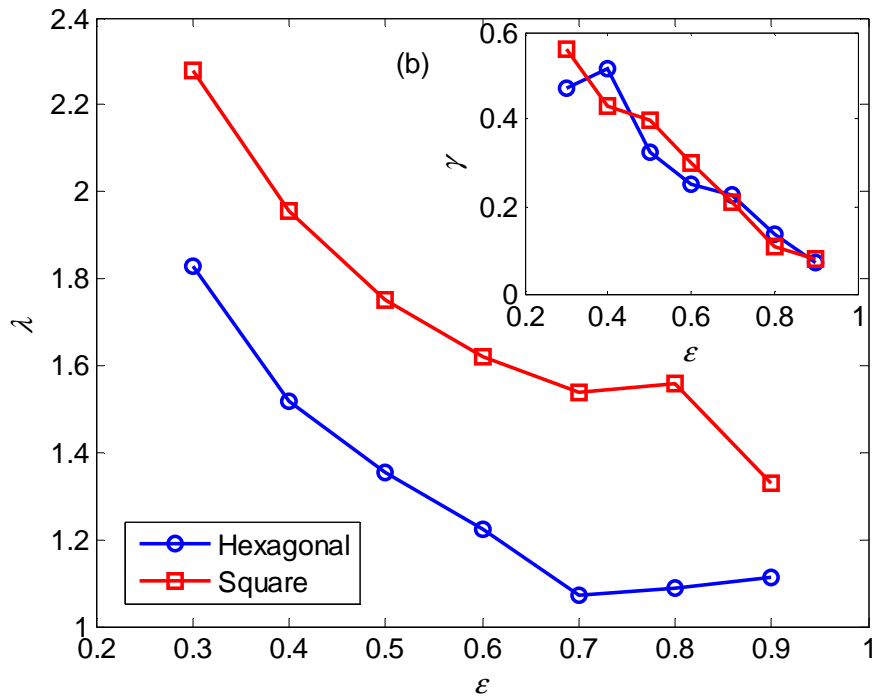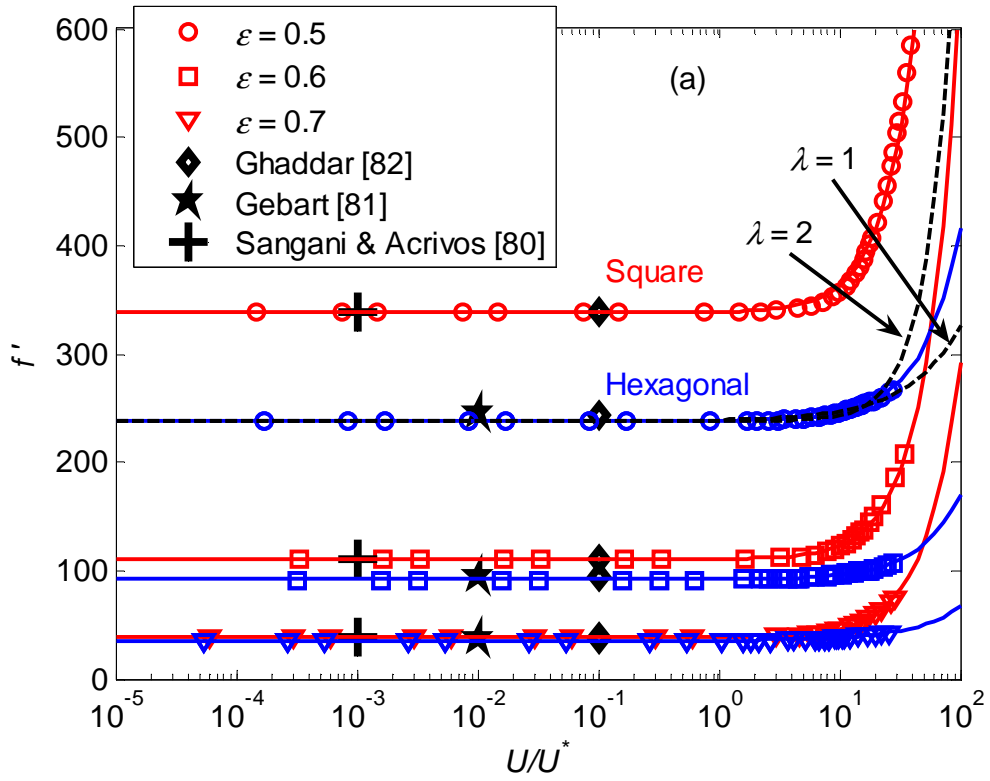
Figure 2 (a): Variation of the modified friction factor as function of the normalized velocity (or Re) for square (red) and hexagonal (blue) configurations (solid lines show

the best least square fit to Eq. (8) and the black dashed lines show the best quadratic ($\lambda = 1$) and cubic ($\lambda = 2$) fits in the range of $10^{-5} < \mathrm{Re} < 30$), symbols show the analytical/numerical data from literature; (b) Inertial coefficients λ and γ as in Eq. (8) plotted against porosity.

3.1.3 Effect of staggered cell angle

In this subsection, the effect of the staggered cell angle, α on the inertial term is discussed. The staggered angle is defined between the diagonal of the unit-cell and flow-direction (horizontal), as shown in Fig. 3(a). In addition to the special cases $\alpha = 45^{\circ}$ and $\alpha = 60^{\circ}$, i.e., square and hexagonal packings, respectively, several other angles are studied.

Fig. 3(b) shows the variation of the modified friction factor as function of normalized velocity for different staggered angles, α at the constant porosity $\varepsilon = 0.7$. Similar to the normalized permeability, the inertial coefficient γ is weakly dependent on the staggered angle in the range of $30^{\circ} < \alpha < 60^{\circ}$. However, λ increases (almost) linearly from $\lambda \cong 1$ at $\alpha = 70$ to $\lambda \cong 2$ at $\alpha = 20$. For $\alpha = 70^{\circ}$ and higher (but lower than the maximum achievable $\alpha_{\max} = \tan^{-1}\left(\pi / \left(2\left(1-\varepsilon\right)\right)\right) \cong 80^{\circ}$), the flow mainly follows a straight line with large superficial velocity and consequently large values of permeability and the transition starts at higher scaled velocities (Re). On the other hand, at $\alpha = 20^{\circ}$ and lower (but larger than the minimum allowable limit $\alpha_{\min} = \tan^{-1}\left(2\left(1-\varepsilon\right)/\pi\right) \cong 11^{\circ}$), the flow is more tortuous and consequently it has lower permeability. At this range, the transition into non-Darcy regimes starts already at smaller superficial velocities.
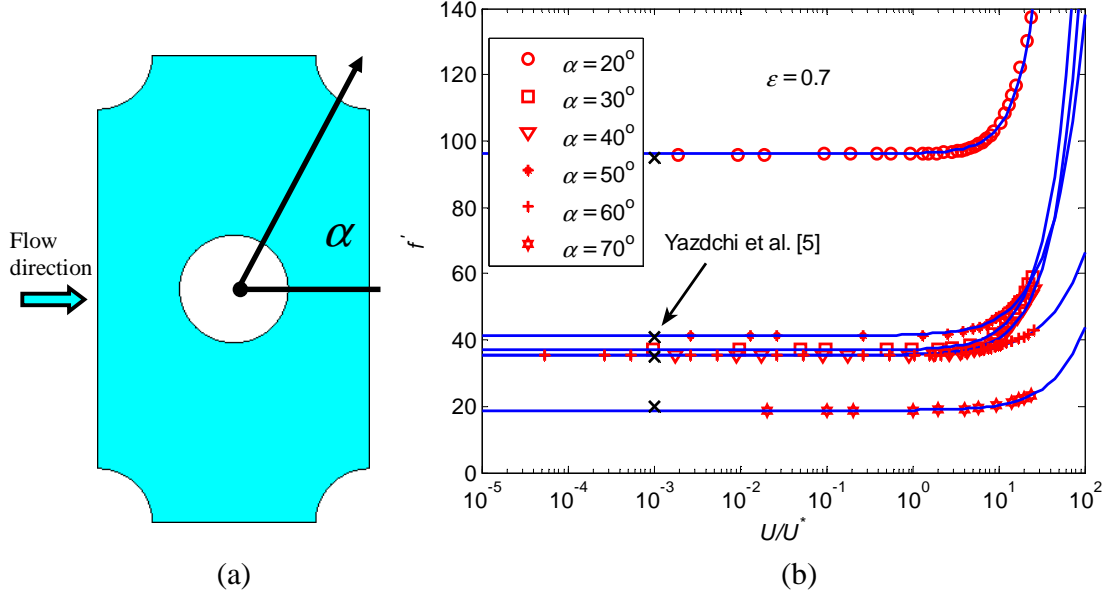
Figure 3: (a) staggered angle α and (b) modified friction factor as function of normalized velocity for different α at porosity $\varepsilon = 0.7$. The solid blue lines show the best least square fit in Eq. (8) in the range of $10^{-5} < \mathrm{Re} < 30$.

3.1.4 Effect of particle shape

In order to study the effect of particle/fibre shapes on the macroscopic permeability and inertial coefficients, the normalization is done with respect to the obstacle length, L_p, which is defined as

$L_p = 4$ area / circumference, with:
$L_p = d$ (for circles), $L_p = c$ (for squares), and $L_p = 4\pi ab / A_L$ (for ellipses) (9)

where d, c, a and $b=a/2$ are the diameter of the circle, the side-length of the square, the major (horizontal) and minor (vertical) lengths of the ellipse, respectively, and A_L is the circumference of the ellipse.

By applying the same procedure as in the previous section, the normalized permeability and inertial coefficients are calculated for different shapes on a square configuration.

Fig. 4 shows the modified friction factor as function of the normalized velocity for different shapes. The circular shape has the lowest and horizontal ellipses the highest normalized permeability. The reason is that, at the same porosity, ellipses are more stretched in the flow direction and therefore the fluid can flow more easily on a straight

18

line through the wider channels. However, at high porosities this effect diminishes (data not shown). Note that, due to the narrower channels, the local maximal velocity is higher for circular shapes, given the same porosity and pressure gradient. However, the superficial (average) velocities for ellipses are larger, leading to higher permeability, than other shapes. For the same reason, the transition to the inertial regime happens earlier for squares, whereas it occurs at higher velocities for ellipses. The values of the inertial coefficients λ, γ and the viscous (normalized permeability, $K^{'}$) term, obtained by least square fitting to Eq. (8), are listed in Table 3. The power λ is not much affected by the shape (maximum variation less than ~10%), however, for squares, the pre-factor γ is ~5 times larger than for ellipses at low porosities. Our numerical results show that, similar to the normalized permeability, the effect of shape on the inertial parameters is less pronounced at high porosities $\left(\varepsilon > 0.9\right)$, not shown here. Establishing a common drag law based on the aspect ratio, sphericity or other shape parameters is still a challenge for future study.

To better understand and explain the flow characteristic in the inertial regime, the patterns of the streamlines for different shapes and the vortices generated behind the obstacle are shown in Fig. 5. The non-Darcy effect occurs because microscopic inertial effects alter the velocity and pressure fields. At the same porosity $\varepsilon = 0.7$ and Reynolds number Re$\cong$10, we observe that for the square shape we have stronger vortices (i.e. those that contribute more to the energy loss) compared to the ellipses in which the wake (or flow separation) zones behind the obstacle is flattened and stretched. These vortices increase in size as the velocity increases and eventually become unsteady and local turbulence occurs. At fixed porosity and pressure gradient, the flow for ellipses is – even though faster in average – less "turbulent" and smoother.

Note that the flow pattern is stationary and symmetric along the horizontal symmetry axis and non-symmetric relative to the vertical axes. The above example implies that the tortuosity (flow path) is one of the key factors in determining the viscous and non-Darcy coefficients (see section 3.2.3 for more details).
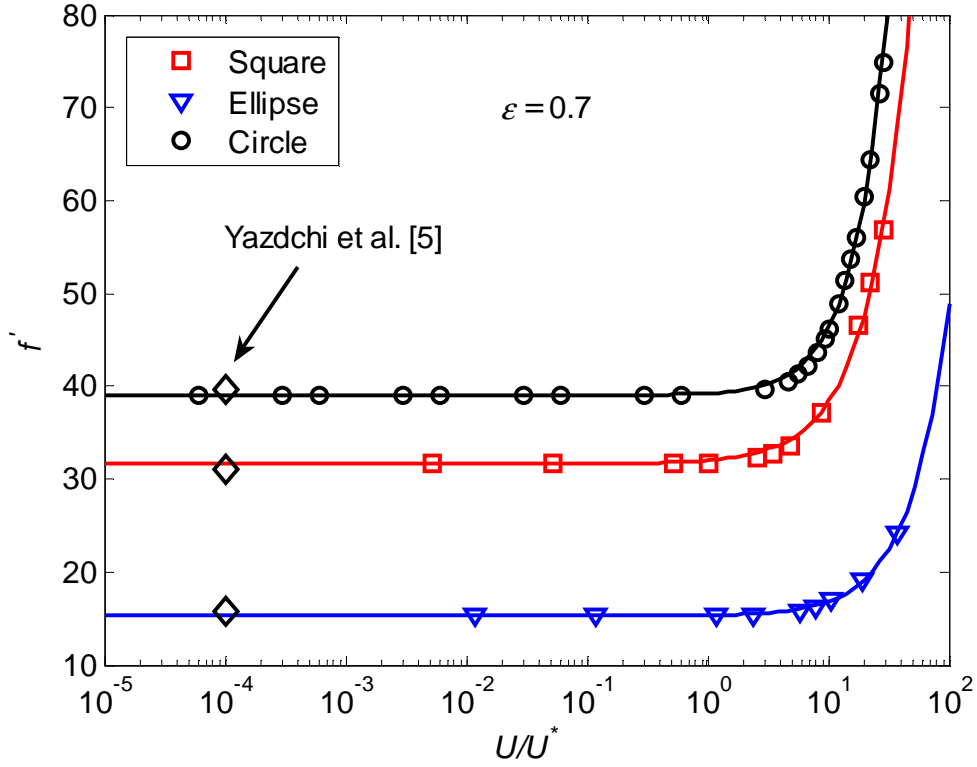
Figure 4: Plot of modified friction factor versus normalized velocity for different shapes at porosity $\varepsilon = 0.7$. The solid lines show the best least square fit in Eq. (8) in the range of $10^{-5} < \text{Re} < 30$.

Table 3: The values of the inertial coefficients λ, γ and viscous (normalized permeability, $K^{'}$ [5]) term, obtained by least square fitting of the FE results into the Eq. (8) in the range of $10^{-5} < \text{Re} < 30$, for different shapes and various porosities.

Shape	Circle			Ellipse			Square		
Porosity, ε	0.7	0.8	0.9	0.7	0.8	0.9	0.7	0.8	0.9
$K^{'} = K / L_p^2$ [5]	0.025	0.077	0.319	0.065	0.147	0.486	0.031	0.091	0.375
λ	1.544	1.561	1.338	1.343	1.436	1.111	1.281	1.342	1.129
γ	0.211	0.113	0.082	0.072	0.058	0.056	0.355	0.168	0.113
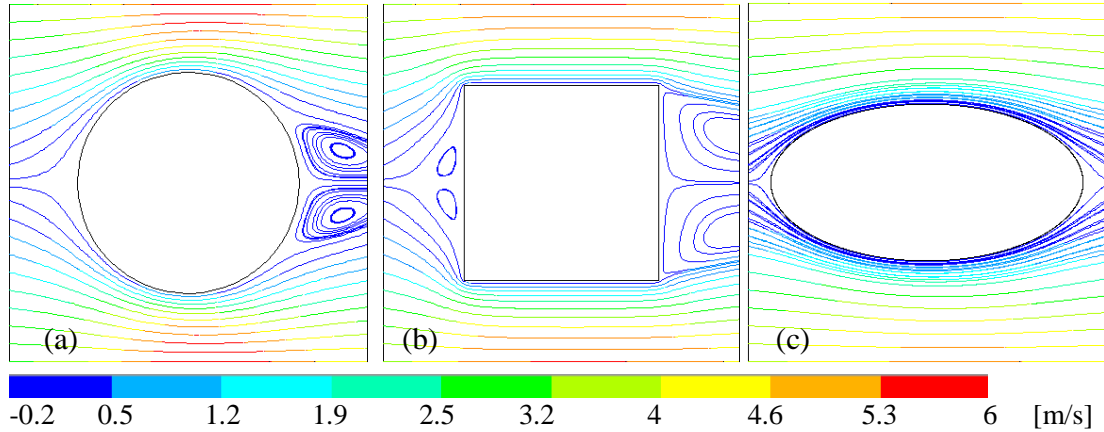
Figure 5: The streamline patterns around (a) circle, (b) square and (c) ellipse of the aspect ratio *a/b*=2 at the constant porosity $\varepsilon = 0.7$ and Re≅10. The color shows the magnitude of the horizontal velocity.

3.2 Structural disorder

Because of the complexity of pore-space geometry, classical numerical methods for solving flows through porous media are typically restricted to ordered and small or periodic domains. However, many realistic porous media are (i) confined with walls, (ii) are not truly two-dimensional, and (iii) possibly contain a degree of randomness (or disorder) at larger length scale that is not adequately represented in too small periodic boundary cells. In this section we focus on (i), as compromise, and investigate the effect of disorder on both viscous and inertial coefficients in a moderately large system with *N*=800 particles/fibres within a channel with walls.

3.2.1 Computational domain and methodology

Fig. 6 shows a 2D representation of *N*=800 randomly distributed fibres, generated by a Monte Carlo (MC) procedure [73], oriented normal to the flow direction at porosity ε =0.6 with minimum inter fibre distance δ_{min}=0.05*d* or dimensionless $\Delta_{min} = \delta_{min} / d = 0.05$. Similar to Chen and Papathanasiou [73], and Yazdchi et al. [5], a minimal distance is needed in 2D to avoid complete blockage. The microstructural parameters, namely the system size, method of generation, homogeneity and isotropy of the structure and their influence on macroscopic permeability have been discussed in [6].

21

At the left and right of the system pressure is set and at the top and bottom walls as well as at the surface of the particles/fibres no-slip boundary conditions are applied. Fibres are assumed to be very long so that a 2D solution can be applied. A typical fine, unstructured and triangular FE mesh is also shown in Fig. 6. The typical range of number of elements is varying from 5×10^5 to some 10^6 depending on the porosity regime. The lower the porosity the more elements are needed in order to resolve the flow in the many narrow channels between the neighboring fibres. Our numerical results show that in all simulations we need at least ~10 rows of elements between neighboring particles to correctly capture the fluid behavior and obtain a converging solution. Details of the comparison of different resolutions are provided in Appendix B. To obtain good statistical accuracy, the permeability values and inertial coefficients were fitted to data averaged over 10 realizations of packings generated by the random MC procedure.
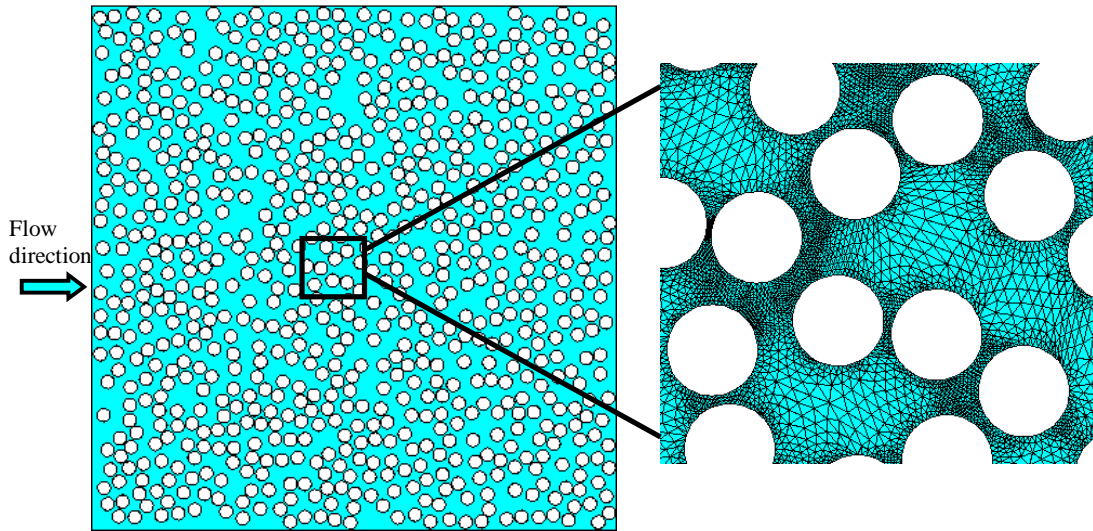
Figure 6: Fibre distributions generated by a Monte Carlo procedure, with N=800 unidirectional cylinders, normal to the flow direction, with minimum inter fibre distance δ_{min}=0.05d at porosity ε =0.6. The zoom shows the fine, unstructured, triangular FE mesh.

Fig. 7(a) shows the variation of the modified friction factor as function of the normalized velocity, U/U^* for disordered configurations at various porosities. As expected, increasing the porosity leads to an increased normalized permeability, $K^{'}$. For Re<3, like

in the ordered hexagonal situations, the normalized friction factor is perfectly fitted by a cubic correction, e.g., for porosities 0.6, 0.7, 0.8, one has $1/K^{'} = 158.8418$, 49.40725, 12.74905, and $\gamma_2 = 0.6569$, 0.5369, 0.2592, respectively. Thus the modified friction factor is considerably larger for low porosity in the random configurations, while the correction quadratic factor ($\lambda=2$) γ_2 is about an order of magnitude larger, implying that the inertial effects occur at much smaller Re numbers already. The relative deviation at Re=1 for the above porosities is 0.004, 0.01 and 0.02, respectively. Thus at Re<<1 Darcy's law holds, yet for Re~1 stationary eddies (dead zones that do not participate in the overall mass-flux) exist mainly due to the geometry of the pores. The gradual deviation from Darcy's law is due to the dynamic growth of pre-existing eddies within the micro-scale flow field and separation of flow in pores where flow diverged. Small deviation between our FE and LB results of Koch & Ladd [15] at creeping flow regime might be due to the difference in minimum inter-fibre distance, resolutions, number of fibers or boundary (periodic/wall) conditions.

Since the quadratic fit deteriorates for Re>0.5-2, we again perform the nonlinear fits to our data up to about Re~30, see Fig. 7(b), where the variations of the inertial coefficients (λ and γ) in Eq. (8) are shown as function of porosity. We observe that for $\varepsilon > 0.45$, unlike for the ordered arrays and similar to the Ergun equation, the power λ is approximately constant and close to unity, whereas the pre-factor γ decreases with increasing porosity. However, at very low porosities ($\varepsilon < 0.45$), λ increases (γ decreases) with decreasing porosity and approaches the expected values ($\lambda \cong 2$) for hexagonal arrays, corresponding to the appearance of ordered zones. Due to the (artificial) gap between fibres/discs, each disc has an effective diameter $d^{*} = d\left(1+\Delta_{\min}\right)$ greater than its actual value, d. With this effective diameter, it is possible to define an effective porosity $\varepsilon^{*} = 1-\left(1-\varepsilon\right)\left(1+\Delta_{\min}\right)^{2}$. Inserting $\Delta_{\min} = 0.05$ and $\varepsilon = 0.45$, the effective transition porosity from disorder to order arrangements is estimated as $\varepsilon^{*} \cong 0.393$. Note that this value is still far above the random close packing limit $\varepsilon_{rcp}^{*} \cong 0.16$ [74], or the minimum hexagonal lattice $\varepsilon_{hex}^{*} \cong 0.0931$, and still above the freezing point $\varepsilon_{f}^{*} \cong 0.309$ [75] or melting point $\varepsilon_{m}^{*} \cong 0.284$ [75]. In fact it indicates that

even small (partial) ordering in the system can drastically affect the transport properties, namely permeability [6] and inertial coefficients of porous media. The comparison of the quality of the proposed power law fit (Eq. (8)) with the quadratic ($\lambda = 1$) and cubic ($\lambda = 2$) fits at different porosities are given in the appendix A.

In appendix D, we present a universal scaling law, valid at all porosities, based on different definitions of Re and friction factor. It is shown that the inertial effect can be better explained as two distinct regimes: (i) cubic correction at Re<1 and (ii) quadratic fit at Re>1, with almost the same accuracy as the proposed power law.
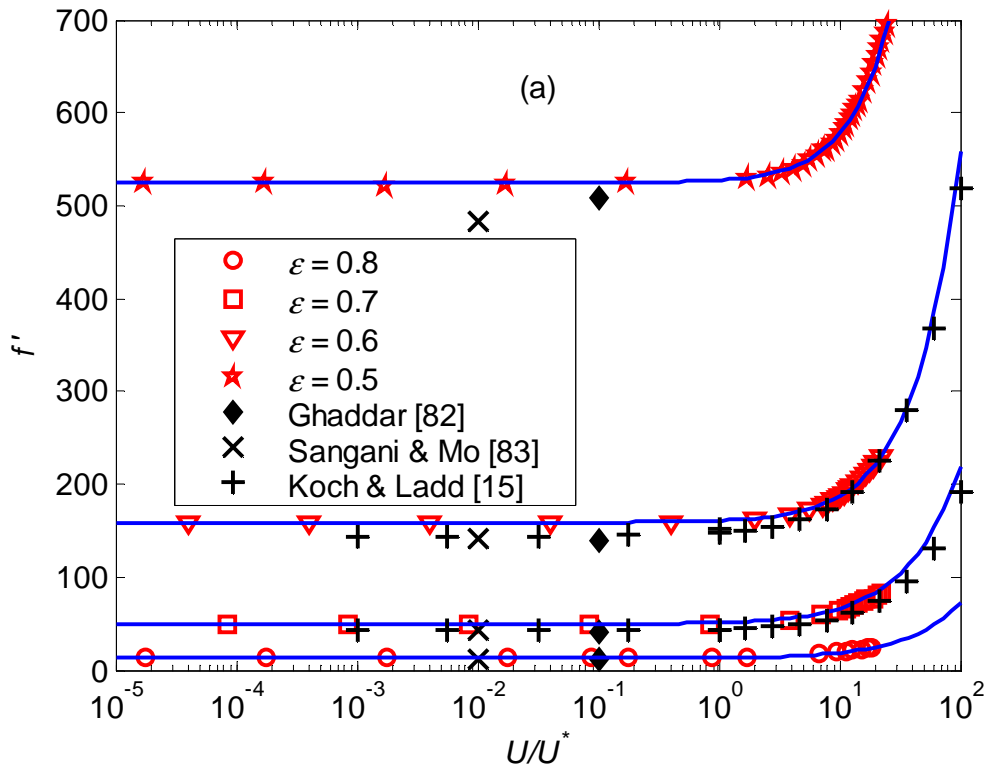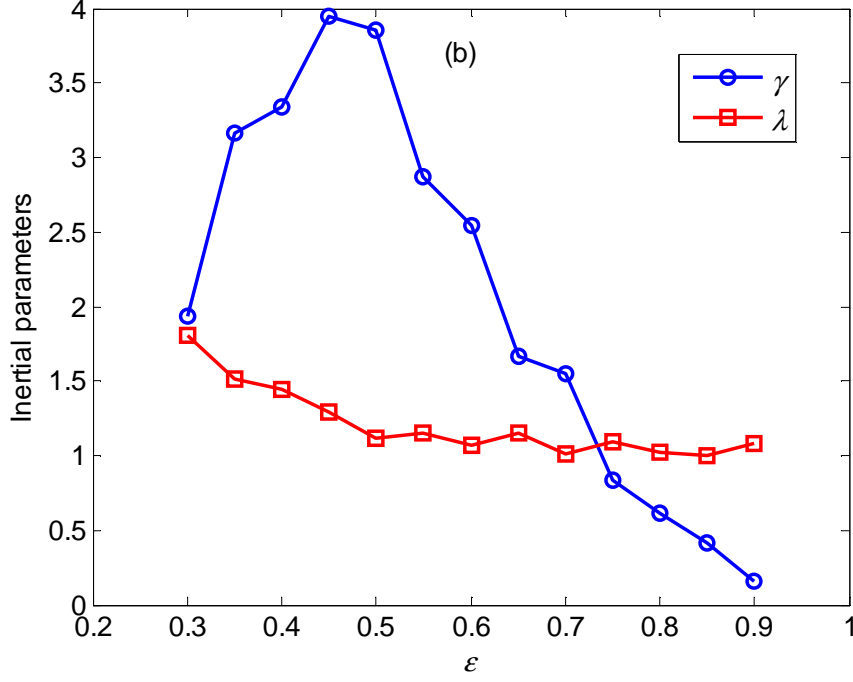
Figure 7: (a) Variation of modified friction factor as function of normalized velocity for disordered media at various porosities[3]. The solid lines show the best least square fit in Eq. (8) in the range of $10^{-5} < \mathrm{Re} < 30$ (b) Inertial parameters as function of porosity.

As mentioned before, most of the available correlations have the similar viscous porosity dependence as the Ergun equation with varying constants ψ_{CK}, where our data lead to a range of $150 < \psi_{CK} < 300$ [76], see next section. Here we are curious to check the quantitative validity of the inertial component of the Ergun equation, i.e. $\gamma = 1.75(1-\varepsilon)/\varepsilon^3$. To this end, we fit our FE results into Eq. (8) assuming constant $\lambda = 1$ (i.e. quadratic correction) for porosities $\varepsilon > 0.45$, i.e. random/disorder co-existence arrangements. Fig. 8 shows the comparison between the inertial coefficient γ, obtained from our FE simulations (blue squares) and from Ergun's equation (red line) at various

---

[3] Note that the numerical values in Koch & Ladd [15] were presented in the form of $f_{KL} = F/(\mu U)$ (F is mean drag per unit length), as function of Re. At steady state, the average drag force multiplied by the cylinder number density, ξ, is equal to the applied pressure gradient, i.e. $\nabla p = \xi F$. Combining this relation with the definition of friction factor in our paper, i.e. Eq. (8), leads to $f^{'} = (4(1-\varepsilon)/\pi) f_{KL}$.

porosities. Astonishingly, the excellent agreement of these curves demonstrates the validity of the inertial component of the Ergun's equation, originally obtained for 3D spherical beds, also for 2D disordered fibrous media.
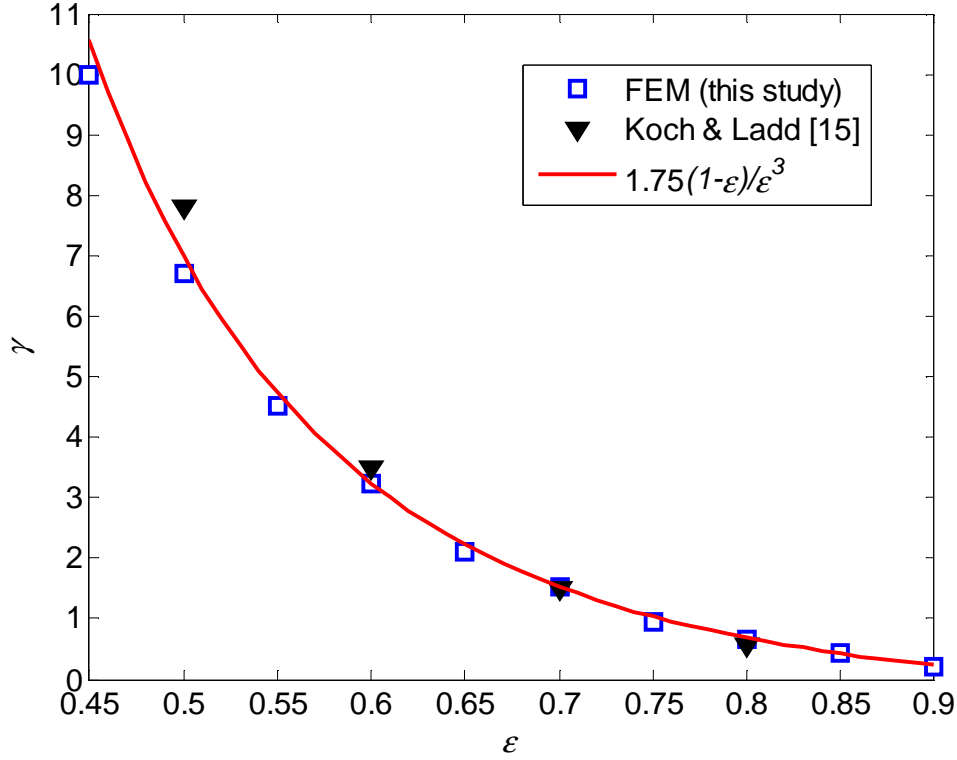

Figure 8: Variation of inertial coefficient γ, obtained from FE simulations (blue squares) and from Ergun equation (red line) at various porosities from disordered configurations.

3.2.2 Different definitions of the Reynolds number

In analyzing flow through porous media, the superficial velocity and pressure drop are typically correlated through the particle friction factor, f_p, which appears as a function of Reynolds number, Re, see Eq. (6). Looking at the literature, several Reynolds numbers for porous media are defined, namely

reference flow Reynolds number: $\quad \text{Re} = \rho U d / \mu$ $\qquad\qquad$ (10)

particle Reynolds number: $\quad\qquad \text{Re}_p = \rho U d / \left((1-\varepsilon)\mu \right)$ $\qquad\qquad$ (11)

modified Reynolds number: $\quad \mathrm{Re}_{\sqrt{k}} = \rho U \sqrt{K} / \mu$ (12)

interstitial Reynolds number: $\quad \mathrm{Re}_i = \rho U d / (\varepsilon \mu)$ (13)

Recently, based on the lubrication effect of the narrow channels, we found a power law relationship between the permeability values obtained from fluid flow simulations and the mean value of 2nd nearest neighbor surface-to-surface fibre distances Δ_{gap} normalized with the fibre diameters [6]. Therefore, another microstructural definition could be the "gap" Reynolds number as $\mathrm{Re}_g = \rho U \Delta_{gap} / \mu \equiv (\Delta_{gap} / d) \mathrm{Re}$, where (Δ_{gap} / d) is a function of porosity [6]. In Appendix D we use this definition to get a universal friction factor-Re_g relation valid at almost all porosities. By increasing the porosity and at the limit of very dilute regime (i.e. $\varepsilon \to 1$ or $d \to 0$), by intuition, the Reynolds number should increase and approach its maximum limit, Re_{max} for the duct flow (i.e. flow between parallel plates). The definitions presented in Eq. (10) and (13) incorrectly approach zero values in this limit. On the other hand, the definition in Eq. (12) contains the macroscopic permeability which, in general, is an unknown quantity- a priori- on the microscopic level. This has motivated us to revisit the definition of the Reynolds number in terms of some measurable quantities of the (random) systems such that a proper trend is recovered also in dilute regimes. A useful, measurable quantity that is frequently used in modeling of porous/fibrous structures is the hydraulic diameter, D_h. When one has obstacles like fibres (or particles) instead of straight pores, the hydraulic diameter can be defined as:

$$D_h = \frac{4\varepsilon V}{S_v} = \frac{4\varepsilon}{(1-\varepsilon)a_v} = \frac{\varepsilon d}{(1-\varepsilon)}, \quad \text{with } a_v = \frac{\text{particle surface}}{\text{particle volume}} = \frac{S_v}{(1-\varepsilon)V} = \frac{4}{d} \quad , \tag{14}$$

with the total volume of the unit cell, V, the total wetted surface, S_v, the specific surface area, a_v. Note that the hydraulic diameter, in this way, is expressed as a function of the measurable quantities porosity and specific surface area. The above value of a_v is for circles (cylinders) – for spheres one has $a_v = 6/d$. Therefore the relation between normalized hydraulic diameter D_h/d and porosity for fibres will reduce to:

$$\frac{D_h}{d} = \frac{\varepsilon}{(1-\varepsilon)}. \tag{15}$$

Using the hydraulic diameter as the characteristic length, we define the pore Reynolds number as

$$\text{Re}_{D_h} = \rho U D_h / \mu,$$ (16)

and combine it with Eq. (15) which leads to

$$\text{Re}_{D_h} = \rho U d \varepsilon / \left(\mu (1-\varepsilon) \right),$$ (17)

For the case of flow between parallel plates (slab flow), separated by distance h_s, the hydraulic diameter is $D_h = 2h_s$ and the superficial velocity, U is related to the pressure gradient as

$$U = -\frac{h_s^2}{12\mu} \nabla p.$$ (18)

Combing Eq. (18) and (16) leads to the maximum Reynolds number $\text{Re}_{\max} = \frac{-\rho h_s^3}{6\mu^2} \nabla p$.

Fig. 9 shows the variation of different definitions of Reynolds numbers as function of porosity at relatively low, constant pressure gradient $\nabla p = 0.0005$ [Pa/m]. The non-Darcy behavior (i.e. high Re numbers) become important due to the combination of high porosity and large pressure gradient. As it is seen, by increasing the porosity the Reynolds numbers (for all the definitions) increase and the flow approaches the inertial regimes even at such a small applied pressure gradient. However, Re (reference Re number) and Re_i (interstitial Re number) will decrease at porosities $\varepsilon > 0.95$ and asymptotically goes to zero. Whereas, the particle Reynolds number (Re_p) and the pore Reynolds number (Re_{D_h}) increases and approaches the maximum $\text{Re}_{\max} = \frac{-\rho h_s^3}{6\mu^2} \nabla p \cong 66$

(though it is a sharp increase from $\text{Re}_{D_h} \cong 0.032$ at $\varepsilon = 0.99$ to $\text{Re}_{D_h} \cong 66$ at $\varepsilon = 1$). We observed that the Re_{D_h} is nicely fitted to the exponential function with the power ~12.5 for the wide range of porosities $\varepsilon < 0.9$. Our numerical results show that this scaling remains valid also at larger applied pressure gradients (data not shown here). For the range of $\varepsilon < 0.8$, the variation of Re_{D_h} is similar to Re_g and $\text{Re}_{D_h}/\text{Re}_g$ is almost constant equal to ~1/6. In Appendix D we use Re_{D_h} or Re_g to get a universal friction factor, valid for all porosities for random configurations.
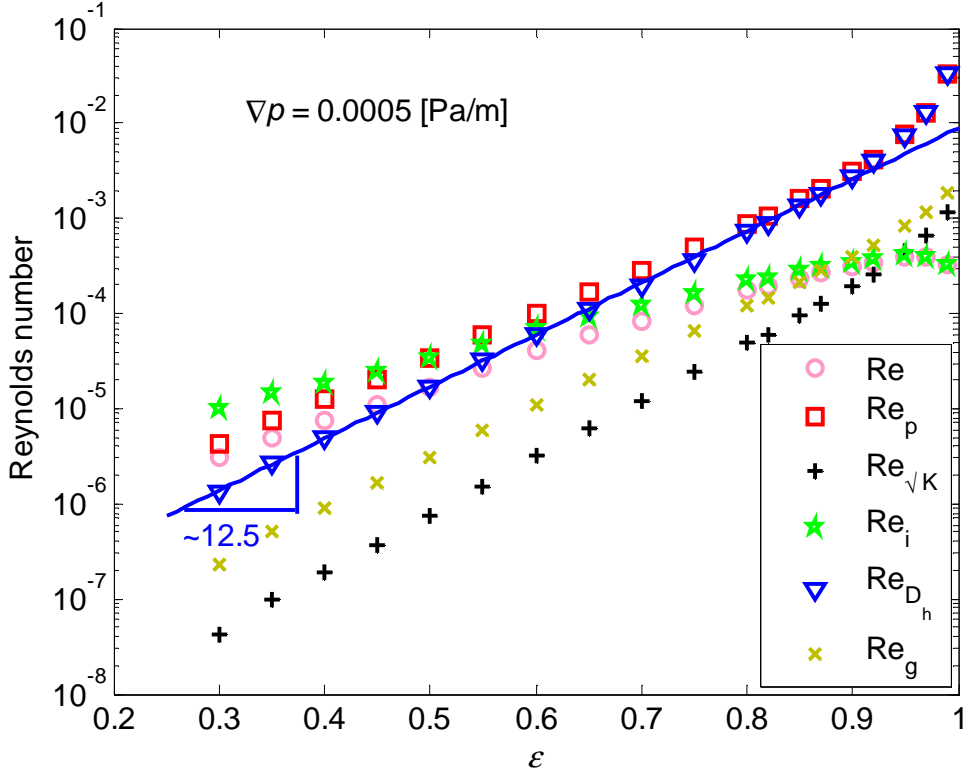
Figure 9: Variation of different definitions of Reynolds number as function of porosity at constant pressure gradient $\nabla p = 0.0005$ [Pa/m] for random configurations.

3.2.3 Effect of inertia on viscous terms ($K^{'}$): Carman-Kozeny (CK) equation

The earliest and most widely applied approach in the porous media literature, for predicting the permeability in Stokes regimes, involves capillary models [77] such as the one that leads to the Carman-Kozeny (CK) equation. The approach is based on the analogy between Poiseuille flow through pipes and pore channels. By applying the Poiseuille equation in terms of the hydraulic diameter, $D_h = \varepsilon d / (1-\varepsilon)$ as $U = -\dfrac{\varepsilon D_h^2}{32\mu}\nabla p$ and combine it with Darcy's law, Eq. (1), the normalized permeability is obtained as

$$K^{'} = \frac{K}{d^2} = \frac{\varepsilon^3}{\psi_{CK}(1-\varepsilon)^2} \tag{19}$$

where ψ_{CK} is the empirically measured CK factor which represents both the shape factor and the deviation of flow direction from that in a duct. It is approximated as ψ_{CK}=180 for

random packed beds of spherical particles [77] or as in Ergun equation (Eq. (4)) ψ_{CK}=150. Reported values of the CK factor for fibrous media are varying between 80 and 320 [78, 79]. The same range of ψ_{CK} has been obtained from the theoretical results of Sangani and Acrivos [80].

The principal limitation of the CK equation is the fact that all geometrical features of the medium are lumped into the CK factor. Even though attempts have been made to introduce microstructural features of the system into the CK equation by suitably modifying the mean hydraulic radius, it is fair to say that, at this stage, microstructural features can be included only semi-empirically through experimental determination of ψ_{CK}. An initial attempt was made by Carman [77] who considered the effect of flow path (tortuosity) on ψ_{CK}. Writing the CK factor in terms of its components, namely the pore shape factor Φ and tortuosity L_e/L

$$\psi_{CK} = \Phi\left(\frac{L_e}{L}\right)^2 \tag{20}$$

The tortuosity, L_e/L is the average effective streamline length, L_e scaled by system length, L. In the original CK equation, for 3D random spherical beds, it was assumed that the tortuosity is constant ($L_e/L = \sqrt{2}$) and Φ=90, which gives us the CK factor as ψ_{CK} =180. However, in a recent study [76] we showed that for fibrous media in the creeping (viscous) regime the tortuosity is not constant and depends on porosity. The effects of several microstructural parameters (namely particle shape, orientation, staggered angle etc) on tortuosity in creeping flow regimes have investigated elsewhere [5, 76]. From our numerical simulations, we extract the average length of several streamlines (using 8 streamlines that divide the total mass in-flux into 9 zones, thus avoiding the center and the edges). By taking the average length of these lines, the tortuosity can be obtained, while by taking the standard deviation of the set of streamlines, the homogeneity of the flow can be judged. The tortuosity is plotted in Fig. 10 as function of normalized velocity at different porosities. Similar to the modified friction factor, the tortuosity is just a function of porosity at creeping flow regimes (horizontal line). However, by turning into inertial regimes, it decreases by increasing the flow rate implying that the fluid flows mainly on a straight line and become less tortuous.
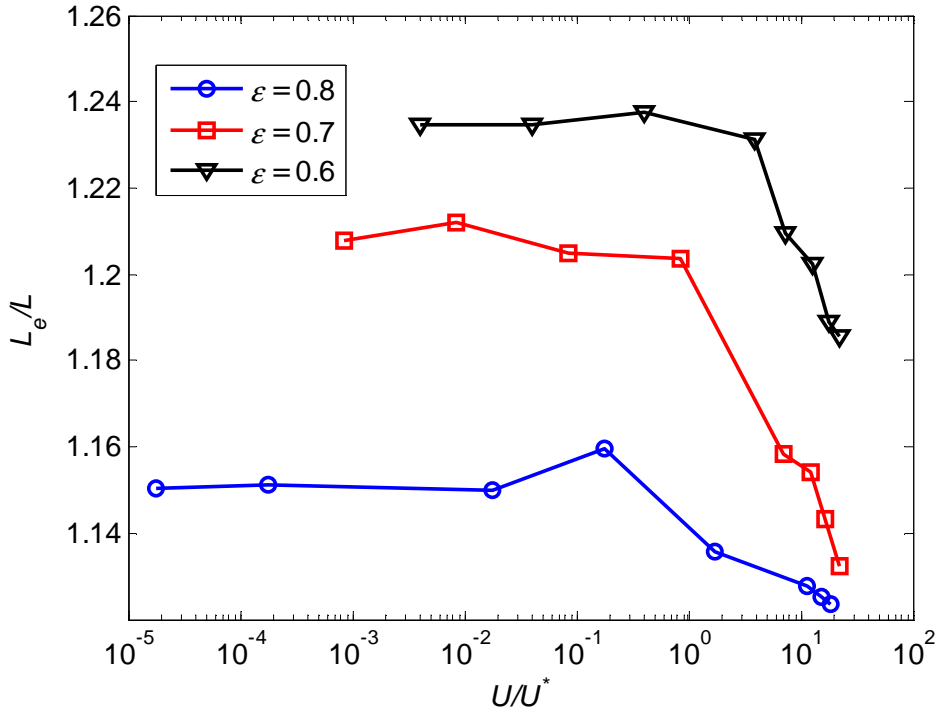
Figure 10: Tortuosity (L_e / L) plotted as function of normalized velocity for different porosities on random configuration.

4. Summary and conclusions

The paper started with an extensive review of published experimental, numerical and theoretical work on the drag law correlations in fluidized beds and porous media with special attention to the intermediate-Re numbers (inertial) regime. Deviation from Darcy's law, for Newtonian, incompressible, stationary flow in homogeneous porous media, was then investigated numerically using FEM. We refer to Darcy's law as linear (in superficial velocity) while different nonlinear corrections for larger Re can be found on the market – from quadratic, intermediate to cubic. Computations were performed on model 2D systems with regularly and randomly distributed, rigid, uniform cylinders/fibres, oriented perpendicular to the flow direction. The effect of several microstructural parameters (namely the shape and structure/arrangement of the fibres) on the macroscopic permeability (viscous drag) and inertial coefficients was investigated

31

first, before we turned to random configurations of cylinders. Major conclusions emerge from the numerical results and can be listed as follows.

For ordered and periodic structures:

- For small Re<3 (threshold varying with porosity, shape, etc.), a cubic correction in velocity ($\lambda = 2$ is the power law for the dimensionless friction factor) works perfectly well, with deviations stronger/earlier for larger porosities – given constant pressure drop.

- Based on the generalized, non-dimensional form of the Forchheimer equation, for larger Re<30, the nonlinear correction to the Darcy drag law is a power law with powers $1 < \lambda < 2$ depending on the porosity and the structure (i.e. square or hexagonal arrays), and with power decreasing from cubic at low porosity towards quadratic at high porosity.

- The viscous and inertial coefficients are not much affected (maximum variation 10%) by the staggered unit cell angle, α in the range of $30^{\circ} < \alpha < 60^{\circ}$. However, λ increases (almost) linearly from $\lambda \cong 1$ at $\alpha = 70^{\circ}$ to $\lambda \cong 2$ at $\alpha = 20^{\circ}$.

- The shape of the particles has a strong effect on both viscous and inertial drag coefficients, especially for porosities lower than approximately 0.9.

For disordered (random) structures:

- For moderate Re, the nonlinear correction to Darcy drag law is well approximated, to first order, by a quadratic term in velocity (i.e. with $\lambda = 1$). The inertial pre-factor $\gamma = 1.75(1-\varepsilon)/\varepsilon^3$ turns out to be very similar to the one used in the Ergun equation, originally derived for 3D spherical packed beds in the range of $\varepsilon > 0.45$ and Re<30. A nonlinear function fits better including also the very small Re data, but best performs a cubic correction up to a critical Re-number, Re_c, and the same with a quadratic correction above Re_c

- With decreasing porosity a structural transition from disordered to ordered packing occurs (for our preparation method) and the inertial coefficients approach values closer to those for the hexagonal lattice.

- The tortuosity (flow path) not only depends on the porosity and the pore structure but also on the fluid velocity (flow regime). At steady state and not fully turbulent

flows, by increasing the porosity or flow rate, the flow becomes faster and less tortuous.

- A microstructural definition of the Reynolds number, Re_g, is based on the mean value of the averaged 2nd nearest neighbor surface-to-surface fibre distances Δ_{gap}. The "gap" Reynolds number $Re_g = \rho U \Delta_{gap} / \mu$, is employed to get the universal friction factor as function of Re_g valid for all Re studied here and in an astonishingly wide range of porosities up to even $\varepsilon \sim 0.9$. After scaling/collapsing all data, both the non-linear fit with non-integer power ($\lambda \cong 1.15$) and the two-regime approach fit the data for Re<30 very well.

Although disorder was investigated in two dimensions, these results provide insights and indicate that similar conclusions might be extended to 3D realistic random porous structures. Further work can now be planned on anisotropic and heterogeneous media and also the study of the fully turbulent regime.

Appendix A.
Comparison of the fit quality for ordered/disordered configurations

The quality of the proposed power law fit for the modified friction factor, Eq. (8), can be evaluated by the relative error, χ defined as:

$$\chi = \left| 1 - \frac{f'_{fit}}{f'_{FEM}} \right| \tag{A.1}$$

The variation of χ as function of $U/U^* \equiv \mathrm{Re}$ using quadratic (blue), cubic (red) and proposed power law fits (black), for (a) square and (b) hexagonal configurations is shown in Fig. A1. The power law fits best to our FE results with maximum discrepancy less than 1%, when the fits are performed in the full range of available data up to Re<30. (Note that the cubic fit performs even better, if not perfect, but only up to Re<3 (varying with porosity)).

The quality factor, χ for random configuration is shown in Fig. A2. Contrary to the case of ordered arrays, the quadratic and power law fits have approximately the same accuracy (maximum discrepancy less than 2%). However, by decreasing the porosity the quadratic correction becomes less accurate.
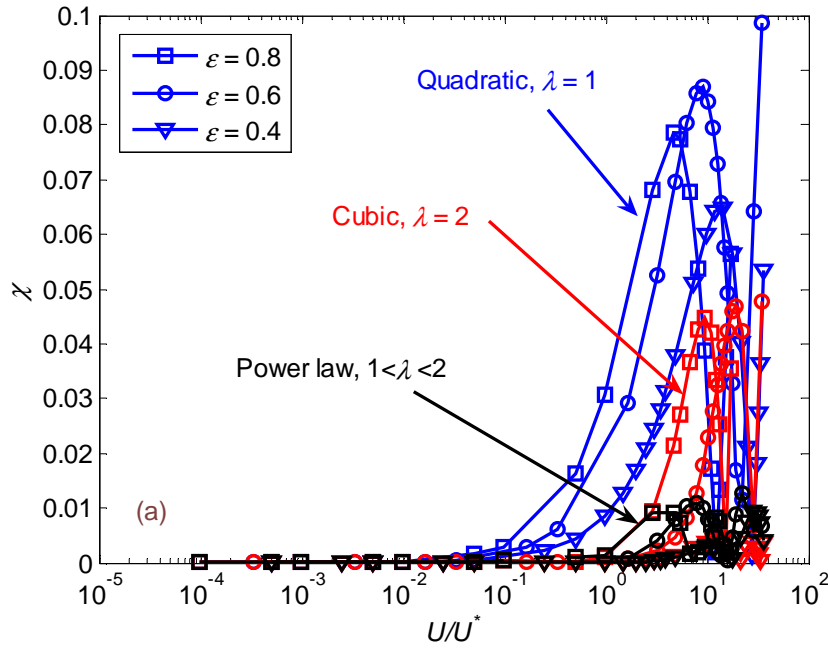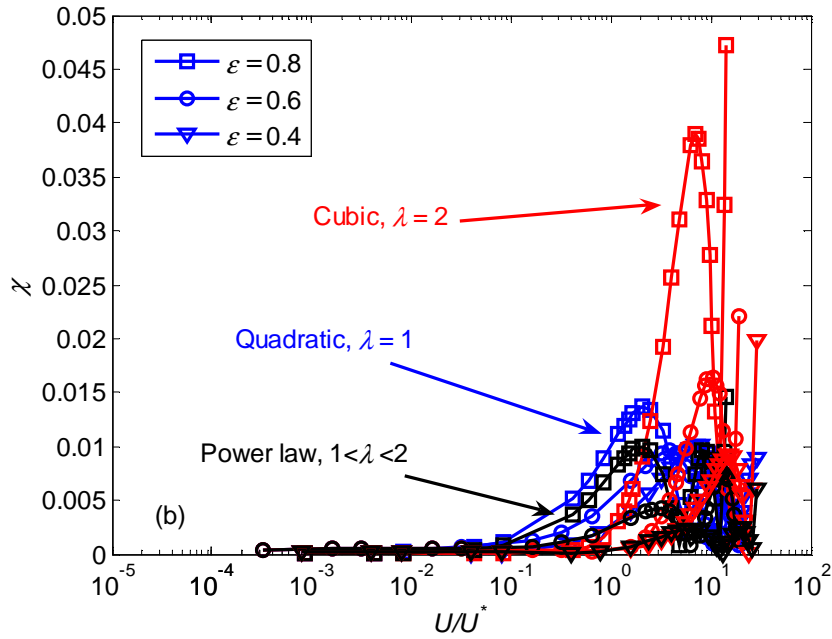
Figure A1: The quality of the quadratic, cubic and proposed power law fit (Eq. (8)) in the range of $10^{-5} < Re < 30$ for (a) square and (b) hexagonal configurations at different porosities.
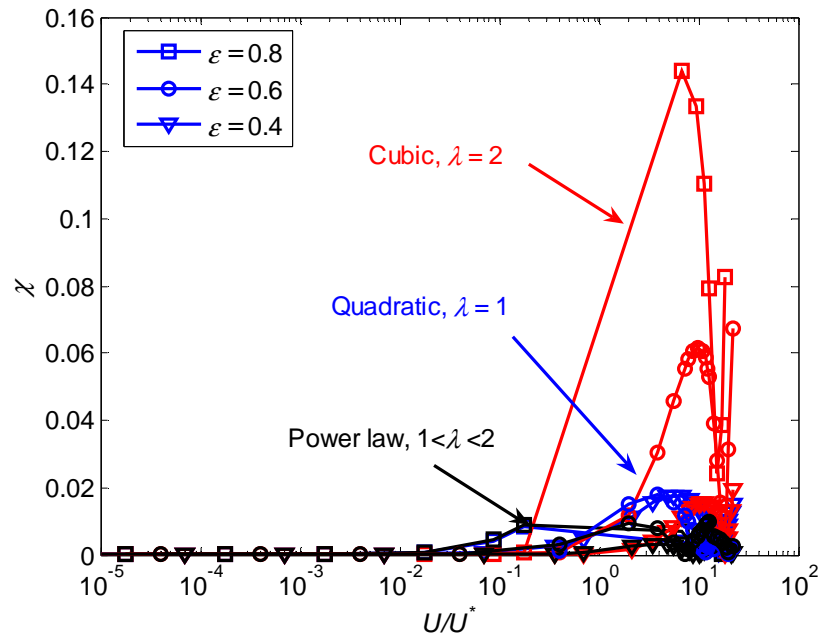

Figure A2: The quality of the quadratic, cubic and proposed power law fit (Eq. (8)) in the range of $10^{-5} < Re < 30$ for random arrangements at various porosities.

Appendix B.

Mesh sensitivity analysis for random arrangements

Due to the difference in scale between domain size and gap size between neighboring fibres, this typically requires local mesh refinement. For different porosities, flow through random fibre arrangements (Fig. 6) was simulated at different mesh resolutions (number of elements, N_e). The dependence of the solution in terms of the calculated friction factor at (a) dense, $\varepsilon = 0.4$, and (b) dilute, $\varepsilon = 0.8$, systems is shown in Fig. B1. The numerical results show that not only the inertial term (more elements are required to reach higher Re numbers), but also the viscous term (normalized permeability K') depends on the resolution, N_e. By increasing the porosity (dilute system) less elements would be sufficient to get a convergent solution.
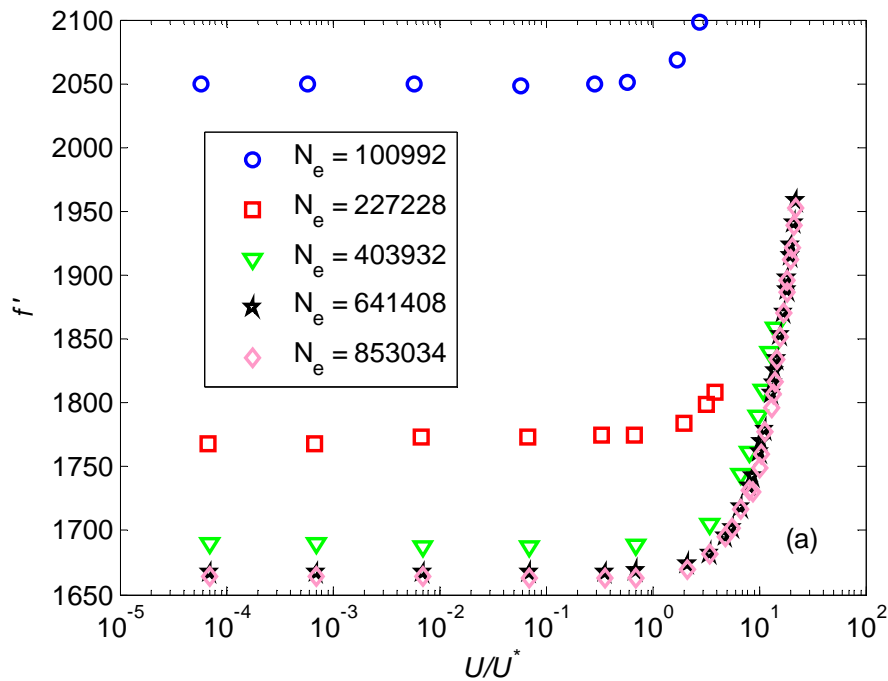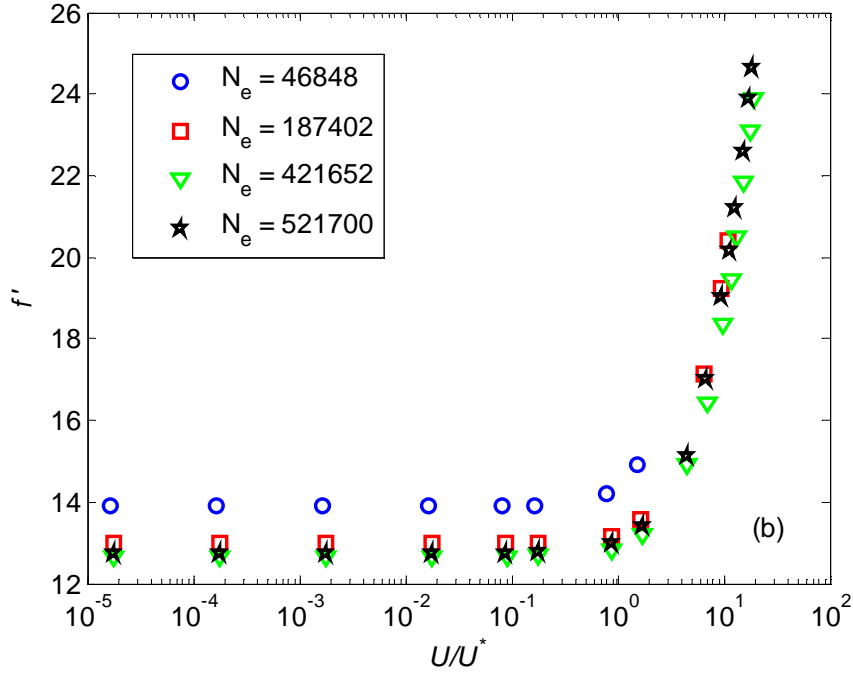
Figure B1: The variation of friction factor as function of Reynolds number $\mathrm{Re} \equiv U/U^{*}$ at porosity (a) $\varepsilon = 0.4$ and (b) $\varepsilon = 0.8$ for different resolution (number of elements, N_e).

Appendix C.

An alternative cubic ($\lambda = 2$) correction fit for the friction factor

The following empirical fit is based on correction of the creep regime (constant f' for $\mathrm{Re} < \mathrm{Re}_c$) with a cubic term ($\lambda = 2$) and fitting the inertial deviation with another correction term, $m(\mathrm{Re})$ for $\mathrm{Re} > \mathrm{Re}_c$. The Re_c is the critical Re number in which the deviation starts. For the case of creeping regime one has the cubic correction for f' as

$$-f' = \frac{1}{K'}\left(1 + \gamma_2 K' \mathrm{Re}^2\right),\tag{C.1}$$

and with the correction at $\mathrm{Re} > \mathrm{Re}_c$ as

$$-f' = \frac{1}{K'}\left(1 + \gamma_2 K' \mathrm{Re}^2\right)m(\mathrm{Re}).\tag{C.2}$$

For the special case of random configuration at $\varepsilon = 0.4$, the numerical fitted values are

$$\begin{cases} K^{'} = 5.9983 \times 10^{-4}, \ \gamma_2 = 1.1816, \ \mathrm{Re}_c = 4.3, \\ m(\mathrm{Re}) = 1 - a_1 (\mathrm{Re} - \mathrm{Re}_c)^2, \ a_1 = 4.3 \times 10^{-4} \end{cases}. \tag{C.3}$$

Fig. C1 shows the variation of friction factor as function of Re=U/U^* together with the proposed fits in Eqs. (C.1), (C.2) and non-integer power law in Eq. (8). The agreement is perfect (better than 99.9%) for $\mathrm{Re} < \mathrm{Re}_c$ using the first correction (Eq. (C.1)) and extends with the same quality up to Re~20 with Eq. (C.2). This indicates that another type of correction is needed in order to improve the prediction for larger Re. Therefore, there is not a single integer power law correction. However, we stop this approach here as the non-integer power law (Eq. (8)) is already a good approximation (maximum discrepancy less than 1%) in wide rage of Re<30.
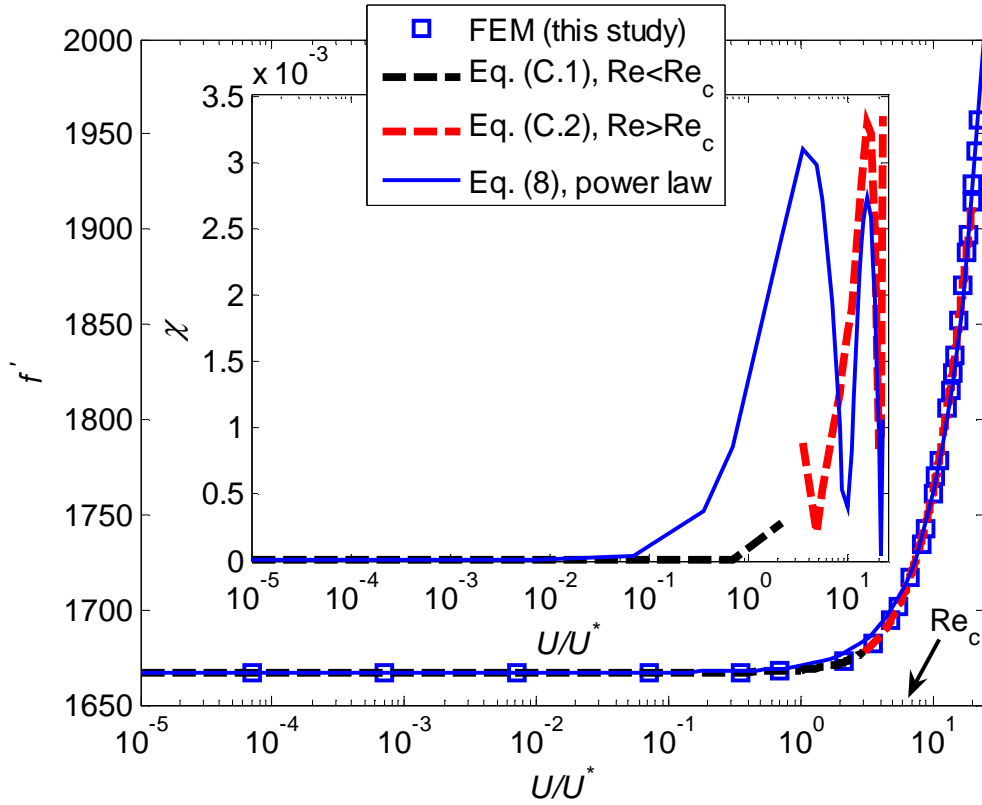

Figure C1: The variation of friction factor as function of Reynolds number $\mathrm{Re} \equiv U / U^*$ for random configuration at porosity $\varepsilon = 0.4$. The dashed and solid lines represent the cubic correction ($\lambda = 2$) fits in Eqs. (C.1), (C.2) and non-integer power law in Eq. (8), respectively. The inset shows the quality of the proposed fits.

Appendix D.

Towards unifying friction factor using different definitions of Re numbers

In this appendix we present unified relations for the friction factor as function of Re_g or Re_{D_h}, valid at a wide range of porosities for random configurations. The non-linear correction in Eq. (8) can be isolated by studying $f^* = -f'K' - 1$, i.e. subtracting the viscous term, as

$$f^* = \gamma K' \, Re_{D_h}^{\lambda} \equiv \gamma K' \left(\frac{\varepsilon}{1-\varepsilon} \right)^{\lambda} Re^{\lambda} \quad \text{or} \quad f^* = \gamma K' \, Re_{g}^{\lambda} \equiv \gamma K' \left(\frac{\Delta_{gap}}{d} \right)^{\lambda} Re^{\lambda}. \quad \text{(D.1)}$$

Note that by replacing Re with Re_{D_h} or Re_g, the values of the fitting power λ would not change. Fig. D1 shows the variation of f^* as function of (a) Re_{D_h} and (b) Re_g at various porosities for the case of random configurations. Using the alternative definitions of Reynolds numbers, i.e. Re_g, the values of f^* at different porosities collapse on a single curve up to astonishingly large porosity, $\varepsilon \sim 0.9$. The weak inertial regime seems to be cubic ($\lambda = 2$), whereas the higher inertial regime fits better to quadratic ($\lambda = 1$) correction. Note that the non-integer power law (Eq. (8)), with $\lambda \cong 1.15$, see the black line in Fig. D1(b), is also fit to our data considering the whole range of Re. Our numerical results show that one can not get such a scaling also for ordered (i.e. square or hexagonal) configurations (data not shown here).
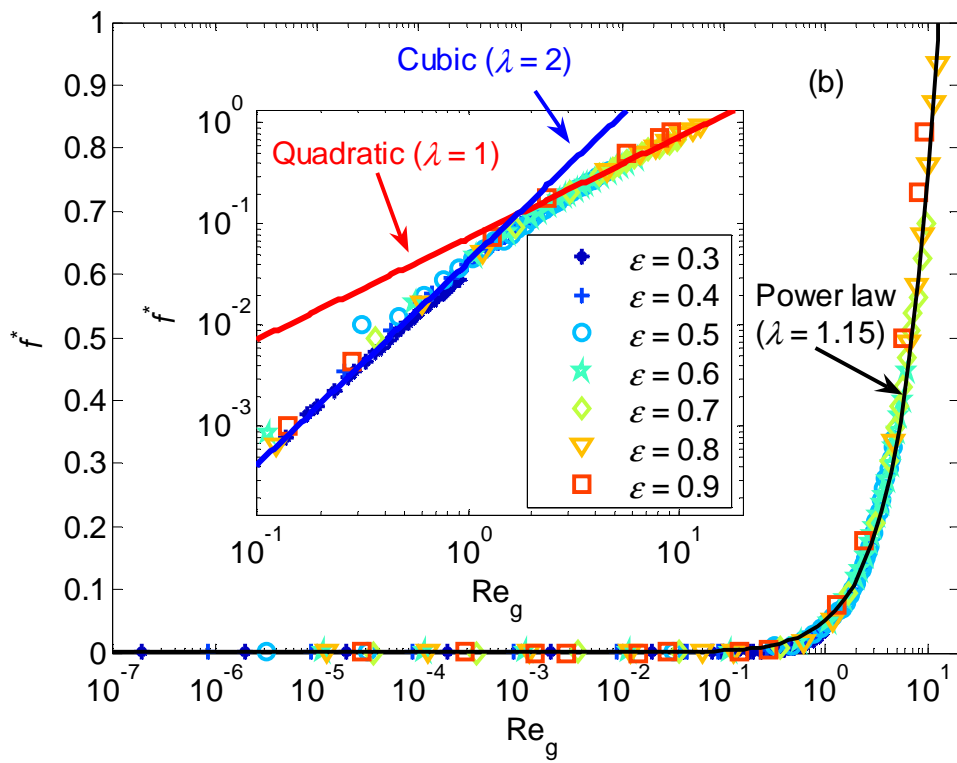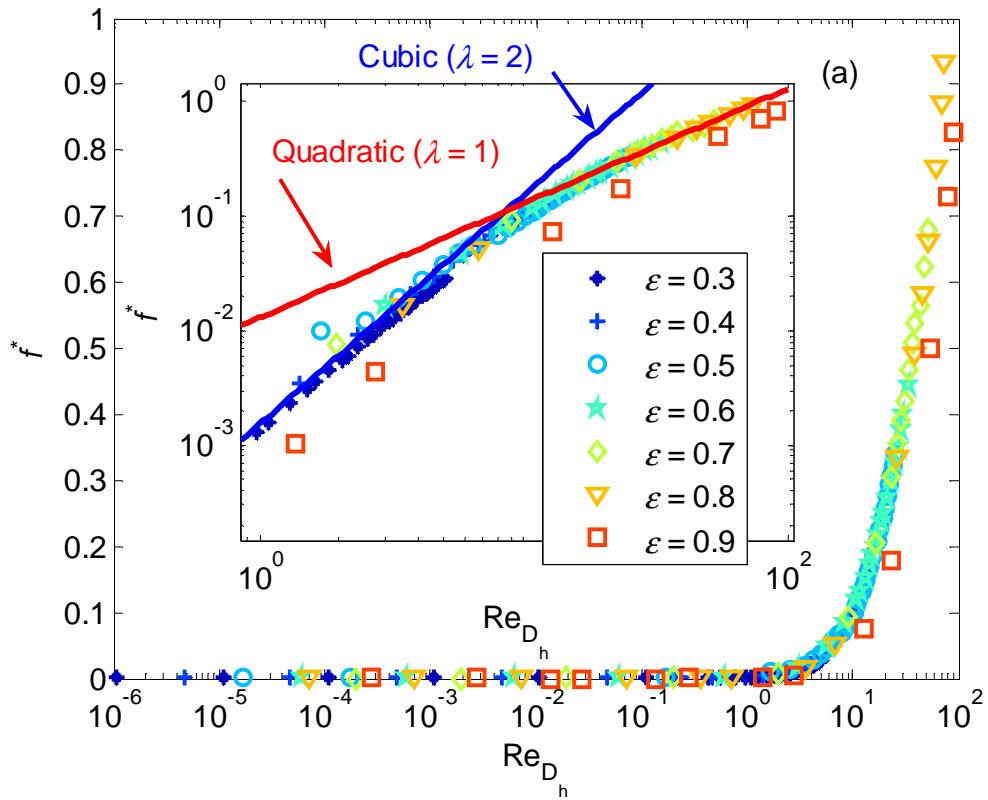
Figure D1: The variation of friction factor as function of (a) hydraulic Reynolds number, Re_{D_h} and (b) gap Reynolds number, Re_g at various porosities for random configurations. The inset shows the zoom. The solid lines show the best fitted cubic and quadratic corrections at weak and high inertial regimes, respectively.

References

[1] N.G. Deen, M. Van Sint Annaland, M.A. Van der Hoef, J.A.M. Kuipers, Review of discrete particle modeling of fluidized beds, Chem. Eng. Sci. 62 (2007) 28-44.

[2] Y. Tsuji, T. Kawaguchi, T. Tanaka, Discrete particle simulation of two dimensional fluidized bed, Powder Technol. 77 (1993) 79-87.

[3] H.P. Zhu, Z.Y. Zhou, R.Y. Yang, A.B. Yu, Discrete particle simulation of particulate systems: A review of major applications and findings, Chem. Eng. Sci. 63 (2008) 5728–70.

[4] H.P. Zhu, Z.Y. Zhou, R.Y. Yang, A.B. Yu, Discrete particle simulation of particulate systems: Theoretical developments, Chem. Eng. Sci. 62 (2007) 3378–96.

[5] K. Yazdchi, S. Srivastava and S. Luding, Microstructural effects on the permeability of periodic fibrous porous media, Int. J. Multiphase Flow 37 (2011) 956-66.

[6] K. Yazdchi, S. Srivastava and S. Luding, Micro-Macro relations for flow through random arrays of cylinders, submitted.

[7] K. Yazdchi, S. Srivastava and S. Luding, On the transition from creeping to inertial flow in arrays of cylinders, Proceedings of IMECE (2010), Vancouver, Canada.

[8] J. L. Lage and B. V. Antohe, Darcy's Experiments and the Deviation to Nonlinear Flow Regime, J Fluids Eng. 122 (2000) 619-25.

[9] S. Whitaker, Flow in porous media I: A theoretical derivation of Darcy's law, Transp. Porous Media 1 (1986) 3-25.

[10] E. Sanchez-Palencia, Non-Homogeneous Media and Vibration Theory, Lecture Notes in Physics 127 (1980).

[11] C.C. Mei, J.-L. Auriault, The effect of weak inertia on flow through a porous medium. J. Fluid Mech. 222 (1991) 647–63.

[12] D.W. Ruth, H. Ma, On the derivation of the Forchheimer equation by means of the averaging theorem, Transp. Porous Med. 7 (1992) 255–264.

[13] F.J. Valdes-Parada, J.A. Ochoa-Tapia, J. Alvarez-Ramirez, Validity of the permeability Carman Kozeny equation: A volume averaging approach, Physica A 388 (2009) 789-98.

[14] J.L. Auriault, Nonsaturated deformable porous media: quasistatics, Transport in Porous Media 2 (1987) 45-64.

[15] D. Koch and A.J.C. Ladd, Moderate Reynolds number flows through periodic and random arrays of aligned cylinders, J. Fluid Mech. 239 (1997) 31–66.

[16] R.J. Hill, D.L. Koch and A.J.C. Ladd, Moderate-Reynolds-number flows in ordered and random arrays of spheres, J. Fluid Mech. 448 (2001) 243–78.

[17] P. Forchheimer, Wasserbewegung durch Boden, Z. Ver. Deutsch. Ing. 45, (1901) 1782.

[18] M. A. Van der Hoef, R. Beetstra and J. A. M. Kuipers, Lattice-Boltzmann simulations of low-Reynolds-number flow past mono- and bidisperse arrays of spheres: results for the permeability and drag force, JFM 528 (2005) 233–254.

[19] A. Narvaez, T. Zauner, F. Raischel, R. Hilfer and J. Harting, Quantitative analysis of numerical estimates for the permeability of porous media from lattice-Boltzmann simulations, J. Stat. Mech. (2010) P11026.

[20] Aydin Nabovati, Edward W. Llewellin, Antonio C.M. Sousa, A general model for the permeability of fibrous porous media based on fluid flow simulations using the lattice Boltzmann method, Composites: Part A 40 (2009) 860–869.

[21] Z. Chai, B. Shi, , J. Lu, , Z. Guo, Non-Darcy flow in disordered porous media: A lattice Boltzmann study, Computers & Fluids 39 (2010) 2069–77.

[22] A. Narvaez, K. Yazdchi, S. Luding and J. Harting, From creeping to inertial flow in porous media: a lattice Boltzmann - Finite Element comparison, submitted.

[23] J. A. Jr. Andrade, U.M.S. Costa, M.P. Almeida, H.A. Makse, and H.E. Stanley, Inertial effects on fluid flow through disordered porous media, Phys. Rev. Lett. 82 (1998) 5249–52.

[24] S. Ergun, Fluid Flow through Packed Columns, Chem. Eng. Prog., 48 (1952) 89-94.

[25] R.B. Bird, W.E. Stewart, E.N. Lightfoot, Transport phenomena, 2nd edn. Wiley, New York, 2002.

[26] T.D. Papathanasiou, B. Markicevic, E.D. Dendy, A computational evaluation of the Ergun and Forchheimer equations for fibrous porous media, Phys. Fluids 13 (2001) 2795–2804.

[27] S. Liu, A. Afacan and J. Masliyah, Steady incompressible laminar flow in porous media, Chem. Eng. Sci. 49 (1994) 3565-86.

[28] G.W. Jackson, D.F. James, Permeability of fibrous porous media, Can J Chem Eng. 64 (1986) 364–74.

[29] G.A. Bokkers, M. van Sint Annaland, J.A.M. Kuipers, Mixing and segregation in a bidisperse gas–solid fluidized bed: a numerical and experimental study, Powder Tech. 140 (2004) 176–86.

[30] C.Y. Wen, and Y.H. Yu, Mechanics of fluidization, AIChE J. 62 (1966) 100-11.

[31] H.C. Brinkman, A calculation of the viscous force exerted by a flowing fluid on a dense swarm of particles, Appl. Sci. Res. A 1 (1949) 27–34.

[32] J.-L. Auriault, On the Domain of Validity of Brinkman's Equation, Transp Porous Med 79 (2009) 215–23.

[33] M. Hassanizadeh, W.G. Gray, General conservation equations for multi-phase systems: 3. Constitutive theory for porous media flow, Adv. Water Res. 3 (1980) 25–40.

[34] T. Giorgi, Derivation of the Forchheimer Law Via Matched Asymptotic Expansions, Transport in Porous Media 29 (1997) 191–206.

[35] M.I.S. Azzam and A.L. Dullien, Flow rate-pressure gradient measurements in periodically nonuniform capillary tubes, AIChEJ 19 (1973) 222–29.

[36] S.M. Hassanizadeh and W.G. Gray, High velocity flow in porous media, Transport in Porous Media 2 (1987) 521–31.

[37] N. Ahmed and D.K. Sunada, 1969, Nonlinear flow in porous media, J. Hydr. Div. ASCE 95 (1969) 1847–57.

[38] S. Whitaker, The Forchheimer equation: a theoretical development, Transp. Porous Med. 25 (1996) 27–61.

[39] D. Lasseux, A. A. Abbasian Arani, and A. Ahmadi, On the stationary macroscopic inertial effects for one phase flow in ordered and disordered porous media, Physics of fluids 23 (2011) 073103.

[40] K.N. Moutsopoulos, I.N.E. Papaspyros, V.A. Tsihrintzis, Experimental investigation of inertial flow processes in porous media, J. of Hydrology 374 (2009) 242-54.

[41] Z. Chen, S.L. Lyons, G. Qin, Derivation of the Forchheimer law via homogenization, Transp. Porous Med. 44 (2001) 325–35.

[42] I.F. MacDonald, M.S. El-Sayed, K. Mow, F.A.L. Dullien, Flow through Porous Media-the Ergun Equation Revisited, Ind. Eng. Chem. Fundam. 18 (1979) 199-208.

[43] T. Farkas, G. Zhong, G. Guiochon, Validity of Darcy's law at low flow-rates in liquid chromatography, J. Chromatogr. A 849 (1999) 35-43.

[44] R.D. Barree, M.W. Conway, Beyond beta factors: A complete model for Darcy, forchheimer, and trans-forchheimer flow in porous media, Proceedings - SPE Annual Technical Conference and Exhibition (2004) 7-14.

[45] A. Bourgeat, E. Marušic-Paloka, A. Mikelic, Weak non-linear corrections for Darcy's Law, Math. Models and Methods Appl. Sci. 6 (1996) 1143–55.

[46] M. Balhoff, A. Mikelic, M.F. Wheeler, Polynomial Filtration Laws for Low Reynolds Number Flows Through Porous Media, Transp. Porous Med. 81 (2010) 35–60.

[47] E. Marušic–Paloka, A. Mikelic, The derivation of a non-linear filtration law including the inertia effects via homogenization, Nonlinear Anal. Theory Methods Appl. 42 (2000) 97–137.

[48] J.-C. Wodié, T. Levy, Correction non linéaire de la loi de Darcy. C.R. Acad. Sci. Paris t.312, Série II (1991) 157–161.

[49] M. Rasoloarijaona, J.-L. Auriault, Non-linear seepage flow through a rigid porous medium, Eur. J. Mech. B Fluids 13 (1994) 177–95.

[50] M. Firdaouss, J.L. Guermond, P. Le Quéré, Nonlinear corrections to Darcy's law at low Reynolds numbers, J. Fluid Mech. 343 (1997) 331–50.

[51] O. Couland, P. Morel, J.P. Caltagirone, Numerical modelling of nonlinear effects in laminar flow through a porous medium, J. Fluid Mech. 190 (1988) 393–407.

[52] H.E. Rose, On the resistance coefficient–Reynolds number relationship for fluid flow through beds of granular materials, Proc. Inst. Mech. Eng. 153 (1945) 154–61.

[53] H.E. Rose and A.M.A. Rizk, Further researches in fluid flow through beds of granular material, Proc. Inst. Mech. Eng., 160 (1949) 493–503.

[54] R.E. Hicks, Pressure drop in packed beds of spheres, Ind. Eng. Chem. Fundam. 9 (1970) 500–502.

[55] J.A. Tallmadge, Packed bed pressure drop - an extension to higher Reynolds numbers, AIChE J. 16 (1970) 1092–93.

[56] J. Sug Lee and K. Ogawa, Pressure drop through packed beds, J. Chem. Eng., 27 (1974) 691–93.

[57] H. Kürten, J. Raasch and H. Rumpf, Beschleunigung eines kugelförmigen Feststoffteilchens im Strömungsfall konstanter Geschwindigkeit, Chem. Ing. Tech. 38 (1966) 941–48.

[58] A. Montillet, E. Akkari and J. Comiti, About a correlating equation for predicting pressure drops through packed beds of spheres in a large of Reynolds numbers, Chem. Eng. Process. 46 (2007) 329–33.

[59] M. Özdinç Çarpinlioglu, E. Özahi, M.Y. Gündogdu, Determination of laminar and turbulent flow ranges through vertical packed beds in terms of particle friction factors, Adv. Powder Tech. 20 (2009) 515–20.

[60] E. Ozahi, M.Y. Gundogdu and Melda Ö. Carpinlioglu, A Modification on Ergun's Correlation for Use in Cylindrical Packed Beds With Non-spherical Particles, Adv. Powder Tech., 19 (2008) 369-81.

[61] L.G. Gibilaro, R. Di Felice, S.P. Waldram, P.U. Foscolo, Generalized friction factor and drag coefficient correlations for fluid-particle interactions, Chem. Eng. Sci. 40 (1985) 1817-23.

[62] S. Benyahia, M. Syamlal, and T.J. O'Brien, Extension of Hill–Koch–Ladd drag correlation over all ranges of Reynolds number and solids volume fraction, Powder Tech. 162 (2006) 166-174.

[63] O. Molerus, Druckverlustgleichung für die Durchströmung von Kugelschüttungen im laminaren und im Übergangsbereich, Chem. Eng. Tech. 49 (1977) 675.

[64] G. Kovács, Seepage Hydraulics, Development in Water Sciences, Elsevier, NY, 1981.

[65] H.R. Kadlec and L.R. Knight, Treatment Wetlands, Lewis Publishers, 1996.

[66] P.U. Foscolo, L.G. Gibilaro and S.P. Waldram, A unified model for particulate expansion of fluidised beds and flow in fixed porous media, Chem. Eng. Sci. 38 (1983) 1251-60.

[67] D. Mehta, M.C. Hawley, Wall effect in packed columns. Ind. Eng. Chem. Proc. Des. Dev. 8 (1969) 280–82.

[68] J.P. Du Plessis, Analytical Quantification of Coefficients in the Ergun Equation for Fluid Friction in a Packed Bed, Transport in Porous Media 16 (1994) 189-207.

[69] W. Reichelt, Zur Berechnung des Druckverlustes einphasig durchströmter Kugel- und Zylinderschüttungen, Chemie-Ingenieur-Technik 44 (1972) 1068-71.

[70] A.R. Martin, C. Saltiel, W. Shyy, Frictional losses and convective heat transfer in sparse, periodic cylinder arrays in cross flow, lnt. J. Heat Mass Transfer., 41 (1998) 2383–97.

[71] A. Tamayol, K. W. Wong, and M. Bahrami, Effects of microstructure on flow properties of fibrous porous media at moderate Reynolds number, Phys. Rev. E 85 (2012) 026318.

[72] Y. Tanino and Heidi M. Nepf, Laboratory Investigation of Mean Drag in a Random Array of Rigid, Emergent Cylinders, J. Hydraul. Eng. 134 (2008) 34-42.

[73] X. Chen, T.D. Papathanasiou, The transverse permeability of disordered fiber arrays: A statistical correlation in terms of the mean nearest inter fiber spacing, Transport in Porous Media 71 (2008) 233-51.

[74] James G. Berryman, Random close packing of hard spheres and disks, Phys. Rev. A 27 (1983) 1053–61.

[75] B. J. Alder and T. E. Wainwright, Phase Transition in Elastic Disks, Phys. Rev. 127 (1962) 359–61.

[76] K. Yazdchi, S. Srivastava and S. Luding, On the validity of the Carman-Kozeny equation in random fibrous media, Particle-Based Methods II - Fundamentals and Applications (2011), 264-273, Barcelona, Spain.

[77] P.C. Carman, Fluid flow through granular beds, Transactions of the Institute of Chem. Eng. 15 (1937) 150–66.

[78] B. Astroem, R. Pipes, S. Advani, On flow through aligned fiber beds and its application to composite processing, J. of Composite Materials 26 (1992) 1351–73.

[79] L. Skartsis, J.L. Kardos and B. Khomami, Resin flow through fiber beds during composite manufacturing processes. Part II. Numerical and experimental studies of Newtonian flow through ideal and actual fiber beds, Polym. Eng. Sci. 32 (1992) 231-39.

[80] A.S. Sangani, A. Acrivos, Slow flow past periodic arrays of cylinders with application to heat transfer, Int. J. Multiphase Flow 3 (1982) 193–206.

[81] B.R. Gebart, Permeability of Unidirectional Reinforcements for RTM, Journal of Composite Materials 26 (1992) 1100–33.

[82] Chahid K. Ghaddar, On the permeability of unidirectional fibrous media: A parallel computational approach, Phys. Fluids 7 (1995) 2563-86.

[83] A.S. Sangani and G. Mo, Inclusion of lubrication forces in dynamic simulations, Phys. Fluids 6 (1994) 1653-62.